General Principles of Cardiac Magnetic Resonance Imaging

1

Mark Alan Fogel

1.1 Introduction

A basic understanding of the underlying principles of cardiovascular magnetic resonance imaging (CMR) and methods used to form images is important if one is to successfully image in clinical practice or research and interpret the data correctly. This section will provide a brief overview of the fundamentals and some techniques in CMR imaging. For more information, the reader is referred to the references in this chapter or the larger textbooks on fundamentals of magnetic resonance imaging as well as other chapters in this book [1].

1.2 Physics and CMR Hardware

The crux of CMR is nuclear magnetic resonance where a signal is emitted by a sample of tissue after radiofrequency energy is applied to it. Note that this signal is emitted by tissue molecules in contrast to X-ray imaging where the tissue or contrast agents attenuate externally applied radiation. At the atomic level, it has been well known that spins and charge distributions of protons and neutrons generate magnetic fields. Only certain nuclei can selectively absorb and subsequently release energy since it requires an odd number of protons or neutrons to exhibit a magnetic moment associated with its net spin. The hydrogen atom is the one utilized in CMR imaging since it consists of a single proton with no neutrons (which gives it a net spin of ½), its large magnetic moment and its abundance in the body (water and fat). Although each magnetic moment of individual hydrogen protons themselves is small, because of the abundance of that atom in the body, the additive effect of the many magnetic moment vectors makes it detectable in CMR.

Generally, the net magnetization of a tissue in the body is zero as there is a random orientation of the individual protons or "spins"; stochastically, the odds greatly favor a zero magnetization. However, when the body is placed in a strong magnetic field (Fig. 1.1) such as 1.5 or 3 T MRI systems (for comparison, the Earth's magnetic field is approximately 0.05 mT at the surface), the spins align themselves with the applied field either parallel or anti-parallel to the field. In addition, the atoms undergo a phenomenon known as precession (such as the motion of a spinning top as it loses its speed) whose axis is based around the direction of the magnetic field (Fig. 1.1a); this precession, described as cycles per second, is described by the most famous equation in CMR and MRI—the Larmor equation, $\omega = \gamma B_0$, where ω is the frequency of precession of protons in an external magnetic field, γ is a constant called gyromagnetic ratio, and B_0 is the external magnetic field (the magnetic field generated by the MRI system). There is a different gyromagnetic ratio for each atom; for hydrogen, it is 42.58 MHz/T which generates a frequency of approximately 64 MHz at 1.5 T (Larmor frequency for a 1.5 T magnet is 1.5 (T) × 42.56 (MHz/T) = 63.8 MHz). When a radiofrequency pulse is applied which just happens to match the Larmor precessional frequency, some of the protons will flip to a high energy state. For protons at field strengths used for CMR, radiofrequencies in range of "very high frequency" or VHF can be used which is non-ionizing, contributing to the inherent safety of MRI when compared to X-rays.

To get from here to how a signal is generated from tissue, two more concepts must be introduced. As mentioned, the hydrogen spins are either in the low or high energy spin states with only slightly more spins in the low energy state. The number of excess spins is directly proportional to the

M. A. Fogel (✉)
Pediatrics (Cardiology) and Radiology, Perelman School of Medicine at The University of Pennsylvania, Philadelphia, PA, USA

Director of Cardiac Magnetic Resonance, The Children's Hospital of Philadelphia, Philadelphia, PA, USA
e-mail: fogel@chop.edu

M. A. Syed, R. H. Mohiaddin (eds.), *Magnetic Resonance Imaging of Congenital Heart Disease*,
https://doi.org/10.1007/978-3-031-29235-4_1

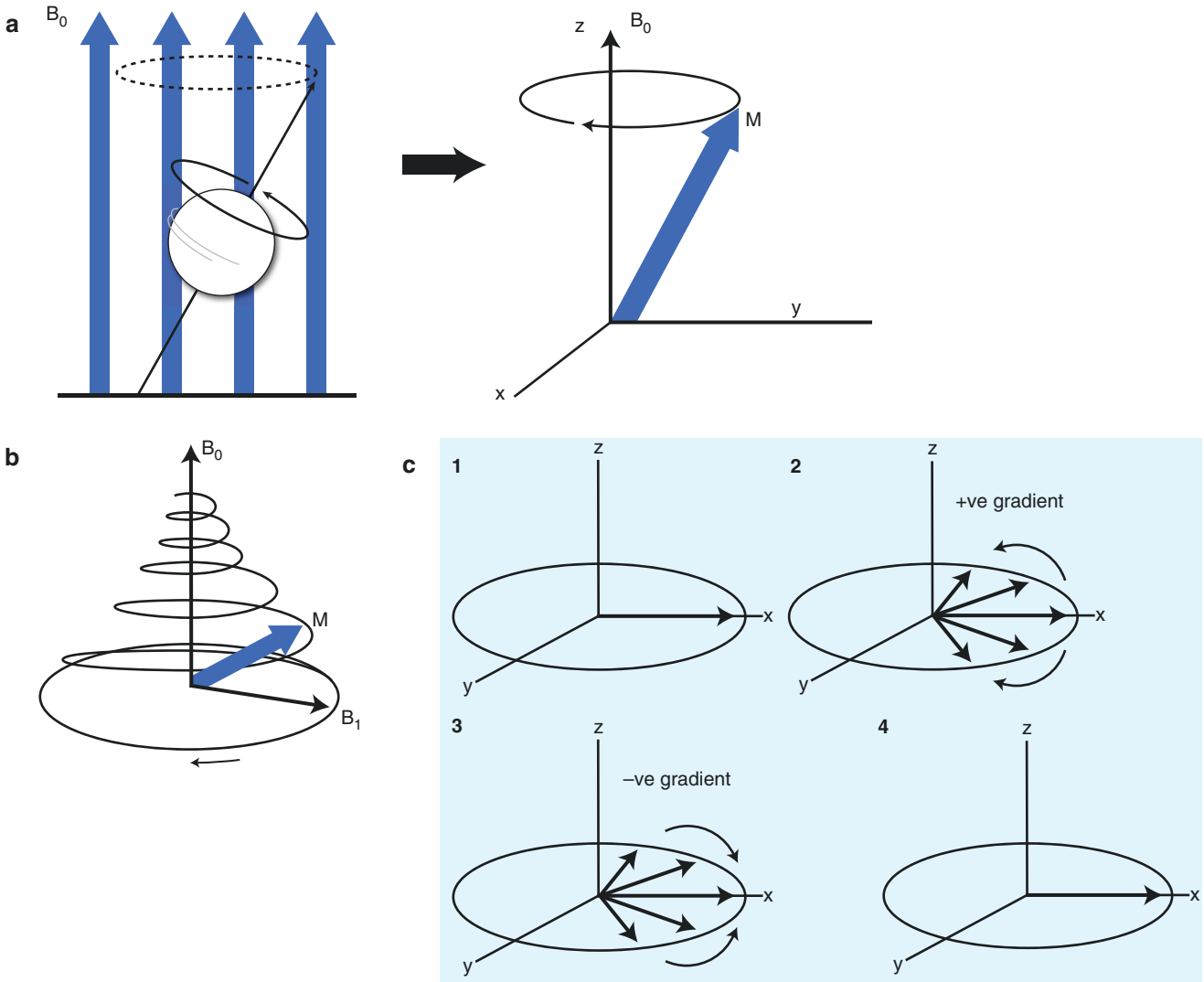

Fig. 1.1 (**a**) Protons spin and process like a top wobbling (left). If the proton is at the (0, 0, 0) coordinate of an *x*, *y*, *z* coordinate system (right), its axis is represented by the blue vector *M* and wobbles around the *z* axis which is in line with B_0 at a frequency ω. (**b**) After energy is inputted into the system, the axis flips (in this particular instance, 90°) and then slowly returns to its original position. (**c**) In (1) the protons are flipped 90 with subsequent "dephasing" of the spins in (2) which can be increased by a gradient (i.e., faster protons and slower protons will separate). In (3), energy can be inputted into the system to flip the protons to an exact mirror image so that the faster spins are not behind the slower spins. Finally, the faster spinning protons catch up to the slower spins to create a large detectable signal (in (4))

total number of spins in the sample and the energy difference between states (Boltzmann equilibrium probability). The formula used to determine this difference is $N^-/N^+ = e^{-E/kT}$ where N^- is the number of spins in high energy state, N^+ is number of spins in the lower energy state, k is Boltzmann's constant (1.3805×10^{-23} J/K), T is the temperature (in Kelvin), and E is the energy difference between the spin states. The second concept is that the energy of a proton (E) is directly proportional to its Larmor frequency υ (in Hz), such that $E = h\upsilon$, where h is Plank's constant ($h = 6.626 \times 10^{-34}$ J s). By substituting into the Larmor equation, this yields the relationship between E and the magnetic field B_0, $E = h\gamma B_0$. When energy is inputted into the system and it matches the energy difference between the lower and higher energy spin states, atoms from the lower energy states get flipped up to the higher energy states. As these atoms then return to the lower energy state, they release energy and this signal, the resonance phenomenon, can be detected (Fig. 1.1b). This is how the MRI signal is generated.

It follows that only those excess spins in the low energy state can be excited to the high energy state and generate the MRI signal. It is amazing that there are only approximately nine more spins in the low energy state compared to the high energy state for each two million spins at 1.5 T! However, one must also realize that since each mL of water contains nearly 10^{23} hydrogen atoms, the Boltzmann distribution

discussed above predicts over 10^{17} spins contributing to the MRI signal in each mL of water! It is interesting to note that the higher the magnetic field strength, the greater the number of excess spins in low versus high energy state; it follows that as the field strength increases, so does the magnitude of the MRI signal. Hence, there is a push by manufacturers to create larger and larger magnetic fields from the 1.5 T fields most commonly used today. Indeed, many 3 T systems have been deployed and 7 T systems have been discussed for clinical use. It should also be noted, as well, that there is research in the opposite direction into lower field systems such as 0.55 T. With modern technology such as advanced gradient systems, pulse sequences, computers, and software, high-quality CMR can be performed at that field strength close to the quality of higher field strength systems [2, 3].

When the radiofrequency energy is applied that matches the Larmor frequency, some of the protons in the low energy state jump up to the high energy level as noted above. This radiofrequency pulse (RF) has a magnetic field itself, B_1, which is perpendicular to the direction of B_0. It is of mT order of magnitude and tilts the longitudinal magnetization (M_z) a certain amount depending upon the duration of the RF pulse and the strength of B_1 field. If an RF pulse is applied to tilt the net magnetization from the longitudinal plane (Z plane) totally to the transverse (XY) plane (called a 90° RF), the transverse component of the net magnetization is the one that will generate an induced voltage in a receiver antenna (the MR signal). The way this occurs is through what is termed "relaxation" where the protons return from their excited state to a low energy state (Fig. 1.1b). The duration of the induced voltage is a function of the time it takes to undergo relaxation and is described by relaxation time constants termed T_1 and T_2 which describe the changes in longitudinal magnetization (M_z) and transverse magnetization (M_{xy}) respectively.

1.2.1 T_1 Relaxation

When the protons are flipped to transverse plane, the M_z component of magnetization decreases to near zero (Fig. 1.1b, c); the time for return of this magnetization M_z after the RF pulse is turned off is measured by the time constant T_1 which is defined as the time necessary to recover 63% of the equilibrium magnetization M_0 after the 90° RF pulse (Fig. 1.2): $M_z(t) = M_0(1 - \exp(-t/T_1))$. Physically, the return of longitudinal magnetization is a function of how fast the spins release their energy to the tissue which is termed the "lattice" hence T_1 being called spin-lattice relaxation. As one might guess, this process depends in part on the physical properties of the tissue where the frequency of precession of the spins needs to overlap the frequencies of the molecules in the lattice. In addition, the process is also dependent on the main magnetic field strength; at higher fields, the frequencies of spins precession increase with less overlap of frequencies in the lattice, resulting in a longer T_1. Water, however, has a frequency range that is large.

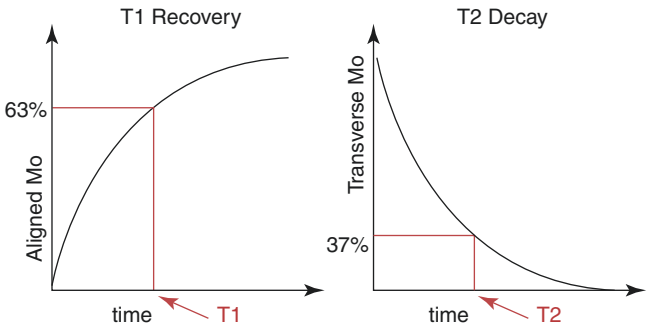

Fig. 1.2 T_1 relaxation or recovery (left) is the return of magnetization M_z, to the equilibrium magnetization M_0; the time constant is defined as recovering to 63%. T_2 relaxation or decay (right) is the decay in the transverse plane

1.2.2 T_2 Relaxation

When the protons are flipped to transverse plane, the M_{xy} component of magnetization becomes maximized as all the protons precess with the same phase, called phase coherence (Fig. 1.1b, c). The spins of each proton in the general vicinity of each other interact with each other, however, and in time, this coherence is lost resulting in a decrease in the net magnetization (Fig. 1.1c) and induced voltage in the receiver antenna. This is appropriately called spin-spin relaxation or transverse relaxation and is measured by the T_2 time constant. The transverse magnetization (M_{xy}) will decay exponentially from M_z by the following formula (Fig. 1.2): $M_{xy}(t) = M_z(0)\exp(-t/T_2)$. The time constant is defined as decaying to 37% of its initial value. This relaxation is highly dependent on the makeup of the tissue; small molecules in a generally unstructured tissue have long T_2 values because fast and rapidly moving spins average out the intrinsic magnetic field inhomogeneities while large molecules in densely packed tissue have shorter T_2 values. Unfortunately, there are other factors responsible for decay of magnetization in the transverse plane; imperfections of the main magnetic field, susceptibility differences between nearby tissues can and do contribute to the loss of phase coherence (Fig. 1.1c). This is measured by the time constant T_2*. In general, T_1 is always greater than T_2 which is always greater than T_2*.

1.2.3 Image Formation

Now that the basic physical properties are defined, the discussion can turn to creating images. To create images, a

magnetic field gradient must be formed. Within the main magnetic field, B_0, all protons precess at the same frequency (Fig. 1.1a). The Larmor equation tells us that this precession is a function of this field strength; by changing the magnetic field ever so slightly by position and time, the precession of the protons can be changed ever so slightly by position and time. Using this information, localization of the MR signal from the precise part of the body can be accomplished and images can be generated. This precision controlled alteration of the magnetic field is created by gradient coils, which generate linear variations in the main magnetic field strength in three orthogonal planes (Figs. 1.1c and 1.3a). By using these coils simultaneously, a linear magnetic field gradient can be generated in any direction. This gradient changes the precession frequency of the protons at precise locations in a linear fashion.

To select a certain plane (slice) in the body (Fig. 1.3b), an RF pulse is applied and it follows that if the RF pulse center frequency is shifted to match a specific location along the gradient, it will selectively excite the protons at that region. A slice of arbitrary thickness, orientation, and location along the direction of the "slice select gradient" can therefore be selectively excited to generate the signal used to form the MR image and the signal detected by the MRI receiver coil will come from the excited slice only (Fig. 1.3b). The amplitude of the signal is directly proportional to its thickness, practically limiting the thickness at approximately 2 mm.

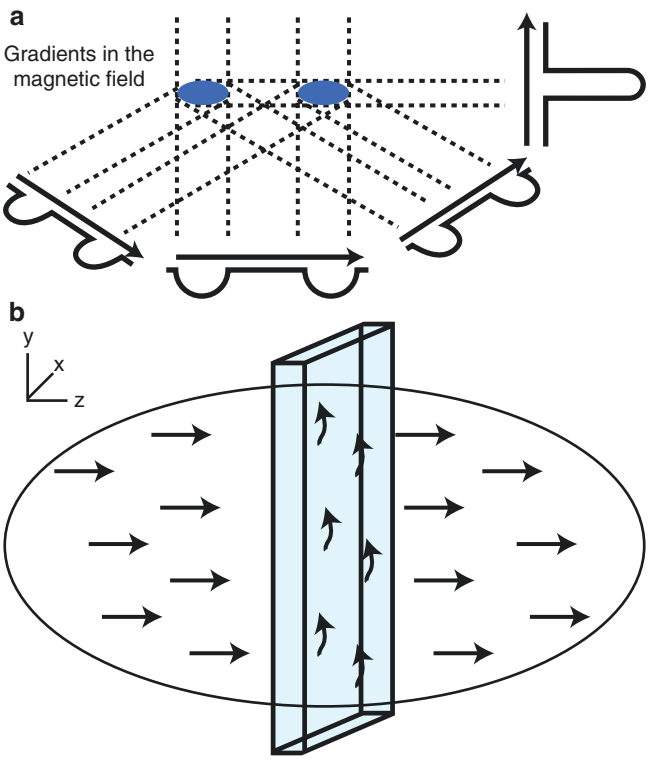

Fig. 1.3 By altering the magnetic field in three orthogonal planes, gradients can isolate a plane in space (**a**). This is accomplished by flipping the protons only in the plane desired (**b**)

After selecting the slice, the image itself needs to be created in two dimensions in the *xy* plane (practically speaking in 2 orthogonal planes of the bore of the magnet—right/left and up/down when looking into the bore). This creates the pixels (2-dimensional picture elements); in 3-dimensional imaging, this is called voxels (3-dimensional volume elements). As with choosing the slice, linear field gradients and the Larmor relationship between field strength and precessional frequency are used to encode spatial location information into the MRI signal. After a slice-selective RF pulse, a linear magnetic field gradient is switched on in one of the in-plane directions of the image, perpendicular to the "slice select gradient"; this gradient changes the precessional frequency in a linear distribution along the gradient direction allowing the identification of every location along the gradient by the frequency of the signal (Fig. 1.3). This is called *frequency encoding*. The MR signal is detected and put through an analog-to-digital converter; remembering that we have encoded the slice and one direction in the plane of the image at this point, the signal is thus the amalgamation of all of these frequencies. Therefore, the signal varies with position, also called its "spatial frequency"; this is called "*k*-space." If one looks at the distribution of the signal, it creates a sinusoidal distribution of phase across the direction of the gradient; this describes a single spatial frequency *kx* (important in phase encoding in the next step). A special mathematical technique called the "Fourier transformation" is used to separate out the individual frequency components in the detected signal, decoding the signal into individual signals coming from locations along the frequency encoding gradient. The Fourier transformation can be used to translate the signal from "*k*-space" to the image and vice versa (Fig. 1.3).

Finally, the third spatial dimension (second in-plane dimension) must also be encoded (if frequency encoding is the "*x*," the "*y*" in the "*xy*" plane must also be created); the technique used is called "phase encoding" (Fig. 1.4) and is also based on the Larmor equation. Phase encoding is accomplished with the application of a number of gradient pulses of differing amplitudes which encode a specific spatial frequency, k_y (Fig. 1.5). This phase encoded gradient pulse is changed to encode a different spatial frequency component prior to each frequency encoding gradient. In this manner, by successive phase encoding pulses, and "*y*" part of the image is built up and a matrix is formed; this matrix is referred to as *k-space*, and the numerous gradient pulses "fill" the *k*-space until the image is complete. The 2-dimensional Fourier transform is utilized to convert the spatial frequencies created by the phase encoding steps into an image (Fig. 1.3). Phase encoding can also be used in the slice direction to

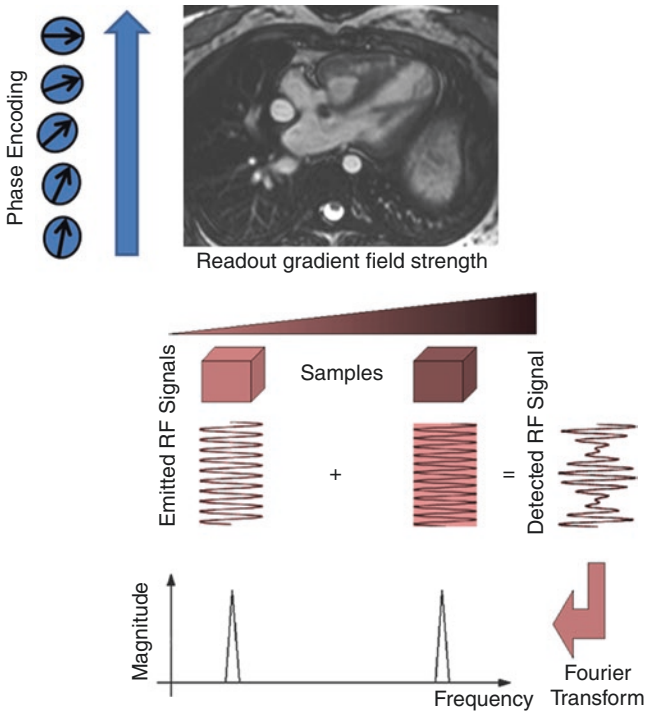

Fig. 1.4 The image is created by a combination of frequency encoding in one direction (in this case, in the *x* plane or the horizontal portion of the image) and phase encoding in the other dimension (in this case, in the *y* plane or the vertical portion of the image). For frequency encoding, a gradient is applied to change the magnetic field in that direction (right triangle). Different frequencies correspond to different positions (different colors and waves on the diagram) which produce a detected radiofrequency (RF) signal which is a combination of all the frequencies of the various positions (rightmost signal). When put through the Fourier transform, signals can be separated into their different positions (lower graph). The vertical portion of the image is created by changing phases of the radiofrequency pulses (phase encoding, see text). The cardiac magnetic resonance image is of a "4-chamber" view of a patient with single ventricle after Fontan

encode thinner slices than possible with the slice selection gradient technique, so-called 3D data acquisition.

1.2.4 MRI Hardware

Once all the components of generating an MR signal are known, it is important to review the equipment needed. There is of course the main magnet (B_0 or B_z field), the RF transmitter coil (B_1 field), the gradient coils (G_x, G_y, G_z fields), and receiver coils which "listen" for the signal. In addition, there are second-order shim coils which are often used to achieve a more homogeneous B_0 field. There are a number of computer systems including those which are used to control the MRI magnetic field-generating units and those used to reconstruct the acquired data. There is also a system which provides an interface for the user and the other systems.

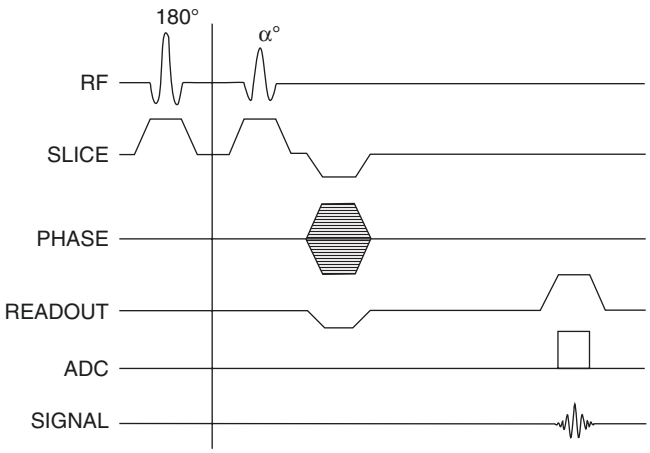

Fig. 1.5 A typical pulse sequence diagram includes (a) when the radiofrequency (RF) pulse is applied (top line) and at times, how much of a flip angle (in this case, 180°), (b) when the slice selection gradient (Gz or slice) is turned on (second line), (c) when the phase encoding gradient (Gy) is turned on (third line), when the frequency encoding gradient (readout or Gx) is turned on (fourth line), and when the analog to digital converter is turned on (fifth line) and the signal is created (sixth line). This is an example of a magnetization prepared gradient echo pulse sequence

1.2.5 Pulse Sequences

This is the sequence of events which control all the various factors involved in the creation of an image. It is important to note that these times are on a microsecond scale and need to be controlled by computer for precise timing. Timing of all the gradients switching on and off, the phase encoding, the RF pulses, the analog to digital converting data sampling, and control of transmitter and receiver operation are all defined by the pulse sequence. As there are a limitless amount of pulse sequences, it is impossible to describe all of them; however, to understand them, a pulse sequence diagram is used which details the timing of each component; a representative pulse sequence diagram is shown in Fig. 1.5. To simplify the concepts, it should be noted that there are five broad concepts with regard to pulse sequences which may be understood to aid in examining many of the pulse sequences in use. They are as follows:

1. *Magnetization preparation* is a technique employed, usually at the beginning of the sequence, which changes the tissue characteristics prior to actually creating the image (Fig. 1.5). T_2 preparation, for example, can be employed to suppress myocardial muscle and is used in visualizing coronary arteries (Fig. 1.6). The inversion recovery technique uses a 180° RF pulse to magnify differences in different tissue characteristics of T_1; the saturation recovery technique uses a 90° RF pulse prior to image. The inversion recovery technique is used in

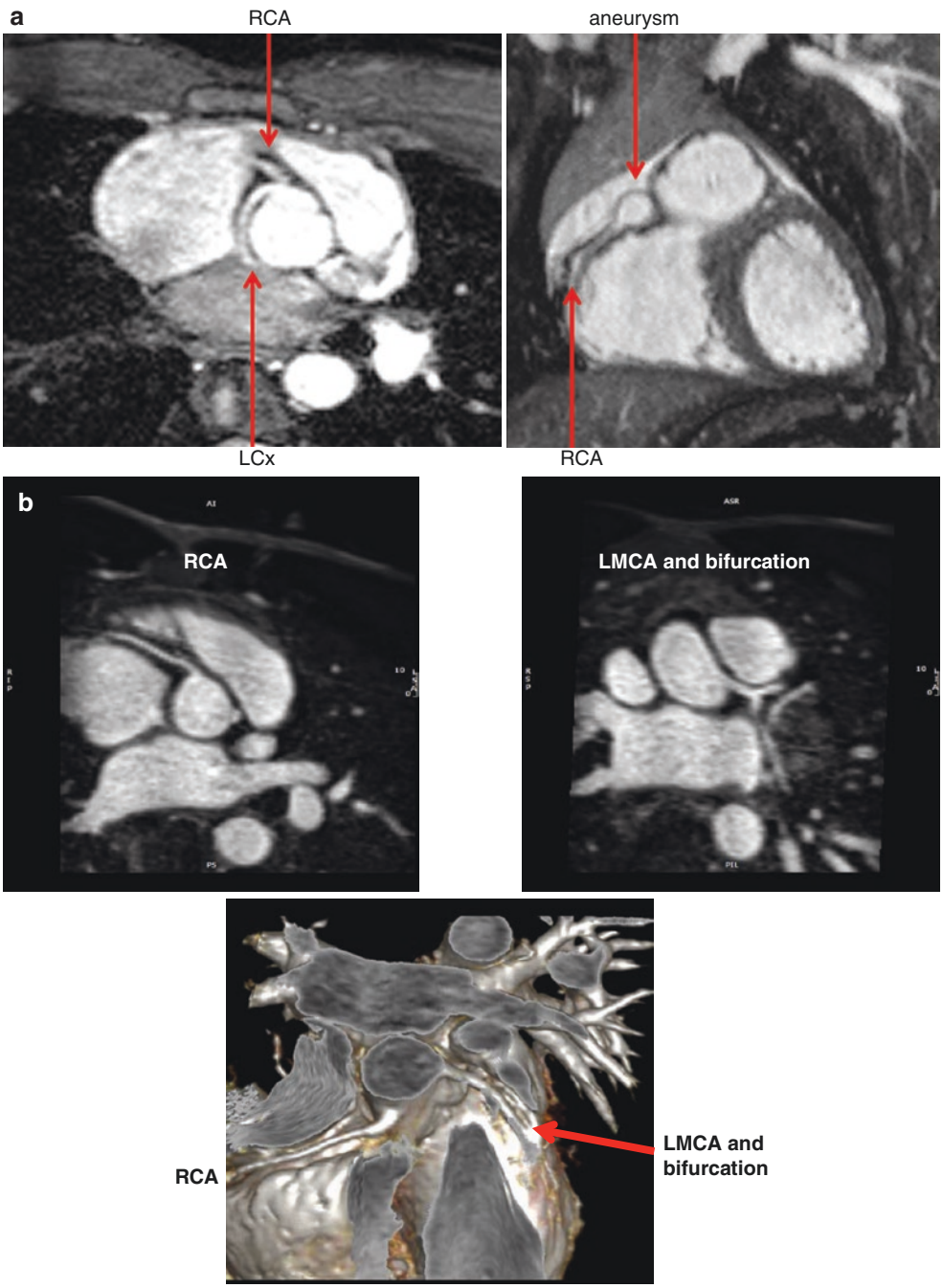

Fig. 1.6 (**a**) T_2 prepared steady-state free precession to visualize coronary arteries. The image on the left demonstrates a right coronary artery (RCA) giving rise to a left circumflex coronary artery (LCx). The image on the right demonstrates a coronary artery aneurysm from Kawasaki's disease from the RCA. (**b**) ECG-gated contrast-enhanced inversion recovery gradient echo imaging of the right (upper left) and left (upper right) coronary arteries with a 3D reconstruction (lower image)

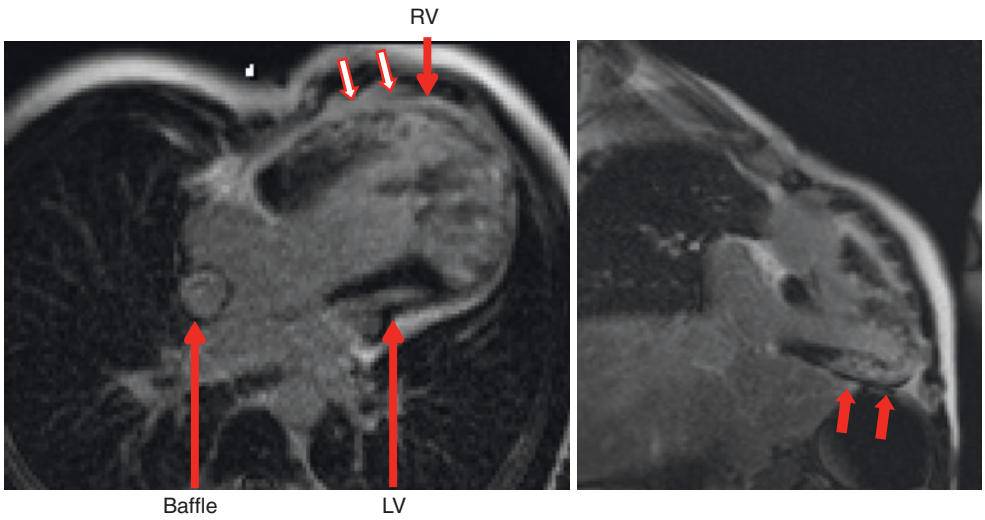

Fig. 1.7 Delayed enhancement imaging from a "4-chamber" (left) and long axis view (right) of a patient with hypoplastic left heart syndrome after Fontan. White arrows in red outline demonstrate some of the areas of myocardial scarring

delayed-enhancement (Fig. 1.7), T_1 mapping as well as dark blood imaging [4] (Fig. 1.8) while saturation recovery is used in T_1 mapping as well as first-pass perfusion imaging (Fig. 1.9).

2. *Echo Formation:* This is the "echo" referred to above and various types of echo formation is used in CMR. An older technique of echo formation which still has applicability today is called spin-echo, which is used most often in dark blood imaging for morphology and tissue characterization (e.g., myocardial edema) (Fig. 1.8). Another technique of echo formation, gradient-echo imaging (Fig. 1.10), is used in a whole host of applications such as:
   (a) Cine imaging for cardiac function including myocardial tagging (Figs. 1.11 and 1.12)
   (b) Assessing valve morphology (Fig. 1.13), valve regurgitation as well as valve or vessel stenosis
   (c) In delayed-enhancement (Figs. 1.7 and 1.10) and first-pass perfusion (Fig. 1.9) for myocardial scarring and myocardial perfusion respectively
   (d) Phase contrast velocity mapping to determine blood flow (Fig. 1.14)

   Gradient echo imaging comes in couple of forms: (a) unbalanced gradient echo imaging and (b) balanced gradient echo imaging also known as steady-state free precession imaging (SSFP) (Figs. 1.15, 1.16, and 1.17). SSFP is more commonly used than the unbalanced gradient echo form due to its high signal to noise, blood to myocardium contrast, and imaging efficiency [5]. Echo-planar imaging is used as a method for perfusion imaging due to its high efficiency.
3. *Filling k-Space:* As noted above, *k*-space is filled with each phase encoding step. Most sequences employ what is known as Cartesian *k*-space sampling, where there is a linear filling of *k*-space with each phase encoding step. There are, however, other methodologies which have come into existence and are used. A "radial" filling of *k*-space has some advantages over Cartesian sampling when it comes to efficiently filling the matrix and has been used in cine imaging [11]. A "spiral" filling of *k*-space trajectory has been utilized for coronary artery imaging, because it has some advantages in speed and most importantly, insensitivity to motion; unfortunately, it is highly sensitive to field inhomogeneities and, therefore, has not gained in popularity. A "radial" filling of *k*-space can be used as well, collecting *k*-space in a series of spokes, with the "golden angle" technique being the most efficient and robust way to do so [12].
4. *Segmentation:* This refers to the number of lines of *k*-space filled per cardiac cycle [13]. If one line of *k*-space is filled per cardiac cycle, that pulse sequence is said to be "segmented"; if all the lines are filled in one cardiac cycle, that pulse sequence is said to be "single-shot" or "non-segmented." There are of course gradations of segmentation between the two and the degree of segmentation is referred to by the number of lines of *k*-space filled per heartbeat (e.g., 3, 5, 7 segments or views, etc.). Any level of segmentation can be used with any of the methods of magnetization preparation, echo formation, or the ways of filling *k*-space. It generally follows that if the more lines of *k*-space filled in a heartbeat, the less time it will take to form the image while the reverse is true with

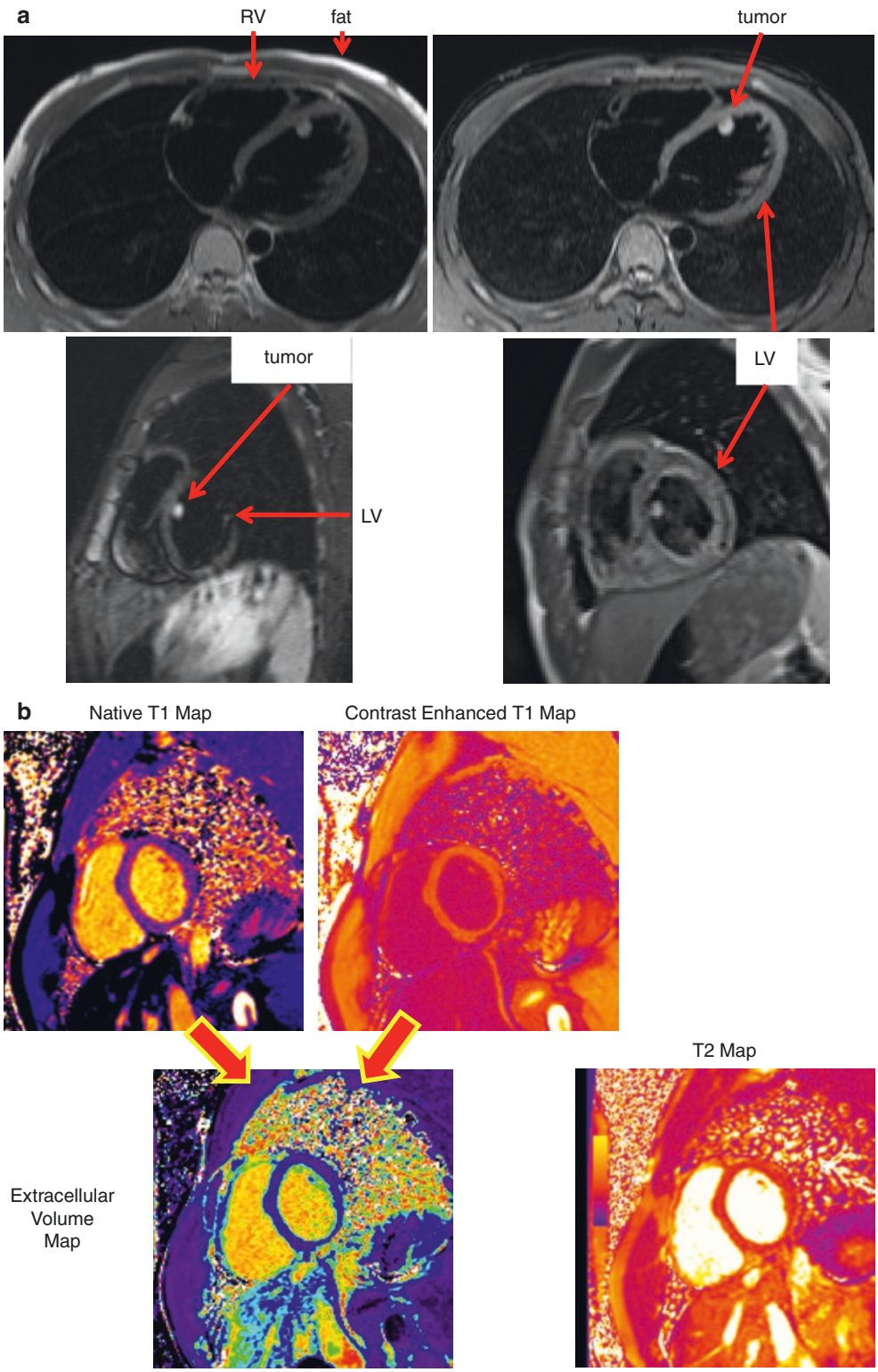

Fig. 1.8 (**a**) Multiparametric mapping. Upper right and left images are T_1 maps before and after gadolinium administration respectively where each pixel's intensity represents T_1 relaxation time. Using the hematocrit, an extracellular volume map can be created (lower left) where each pixel's signal intensity represents the extracellular volume percentage. The lower right panel is a T_2 map where each pixel's intensity represents T_2 relaxation time. (**b**) Dark blood imaging in a patient with a left ventricular hemangioma (tumor). The upper left panel is a dark blood T_1-weighted image of the tumor demonstrating slight hyperenhancement; note the fat in the chest wall. The upper right panel is the same dark blood T_1-weighted image with a "fat saturation" pulse applied prior to imaging (prepulse). Note how the fat in the chest wall is not present in this image because the prepulse destroyed all the spins of the fat; however, the tumor is still present, indicating there are no fatty elements in the tumor (it is not a lipoma). The lower left panel demonstrates hyperenhancement on T_1-weighted imaging after gadolinium administration. The lower right image is a T_2-weighted image with fat saturation demonstrating hyperenhancement indicating increased water content

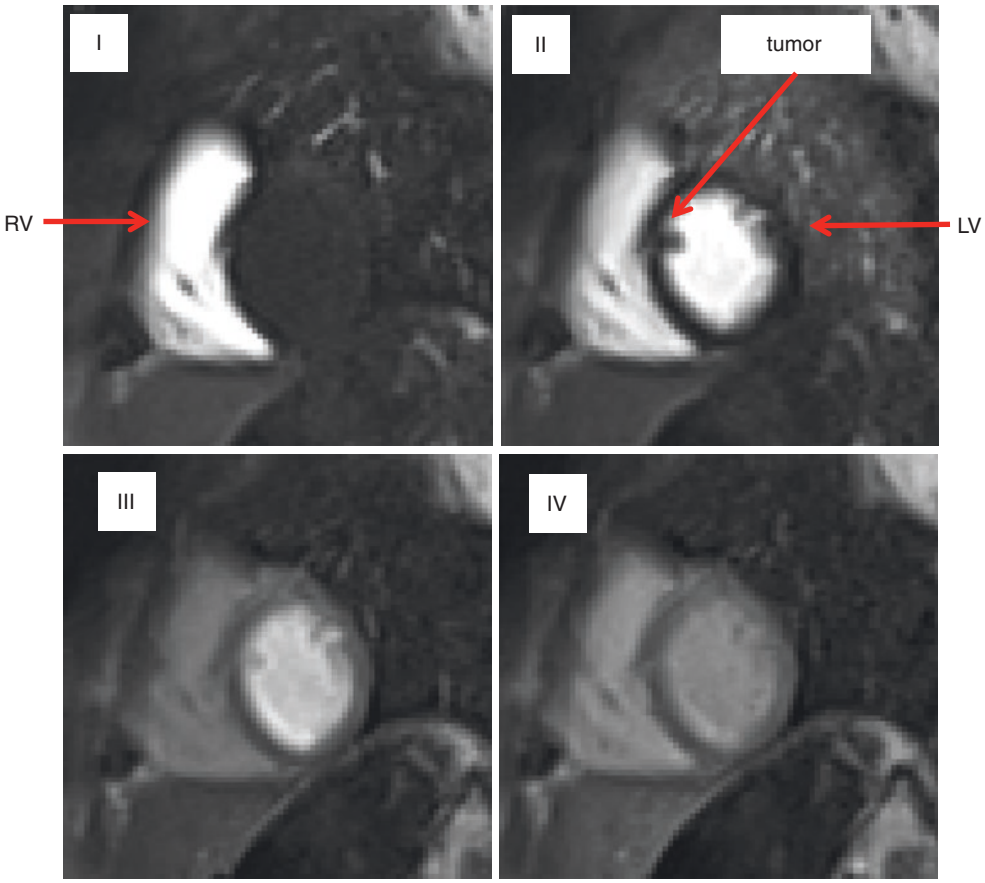

Fig. 1.9 Perfusion imaging in the patient in Fig. 1.8 with a left ventricular hemangioma (tumor). Four frames during the first pass myocardial perfusion imaging demonstrate contrast in the right ventricular (RV) cavity (I), the left ventricular (LV) cavity (II) where the tumor can be seen, and phases III and IV where the contrast enters the LV myocardium. Note how the tumor becomes signal intense in III and IV; so much so that it is indistinguishable from the cavity (somewhat in III and indistinguishable in IV). The tumor can be visualized in II as the contrast is in the cavity but not in the myocardium where presumably the tumor receives its blood supply from

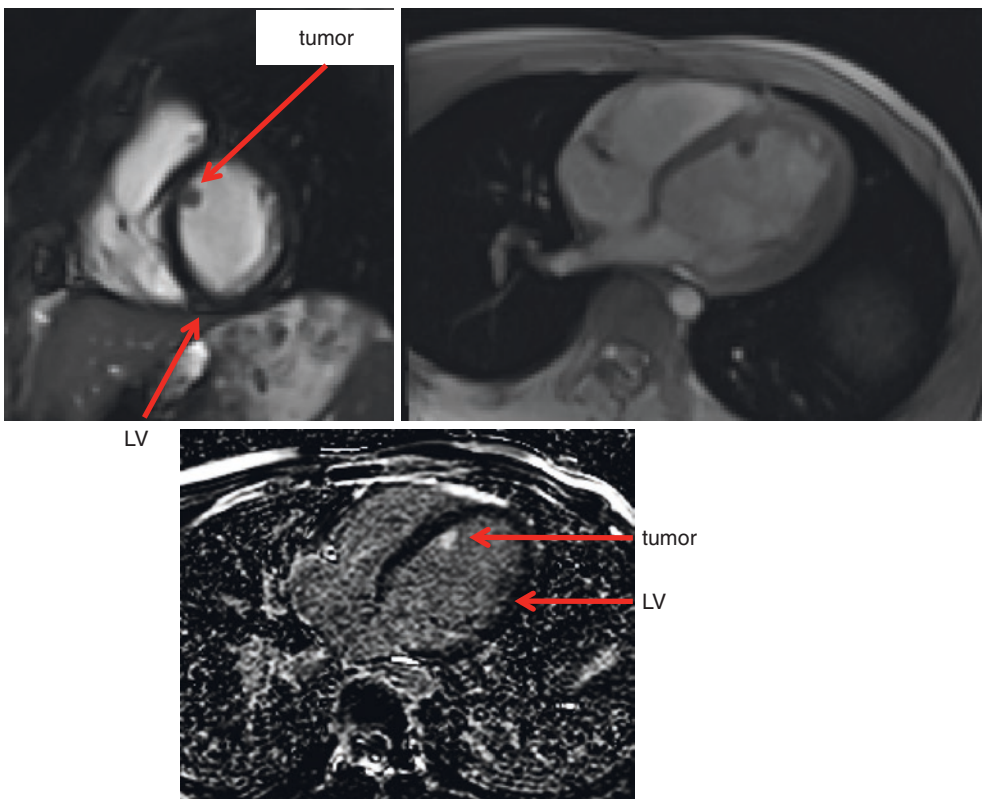

Fig. 1.10 Tissue characterization in the patient in Figs. 1.8 and 1.9 with a left ventricular hemangioma. The upper left panel is a steady-state free precession image in short axis clearly showing the spherical tumor while the upper right panel is an axial gradient echo sequence also clearly showing the tumor. Note the tumor is isointense with cardiac muscle on steady-state free precession and the hypoenhancement on gradient echo imaging. The lower image is a delayed enhancement image of the tumor demonstrating hyperenhancement

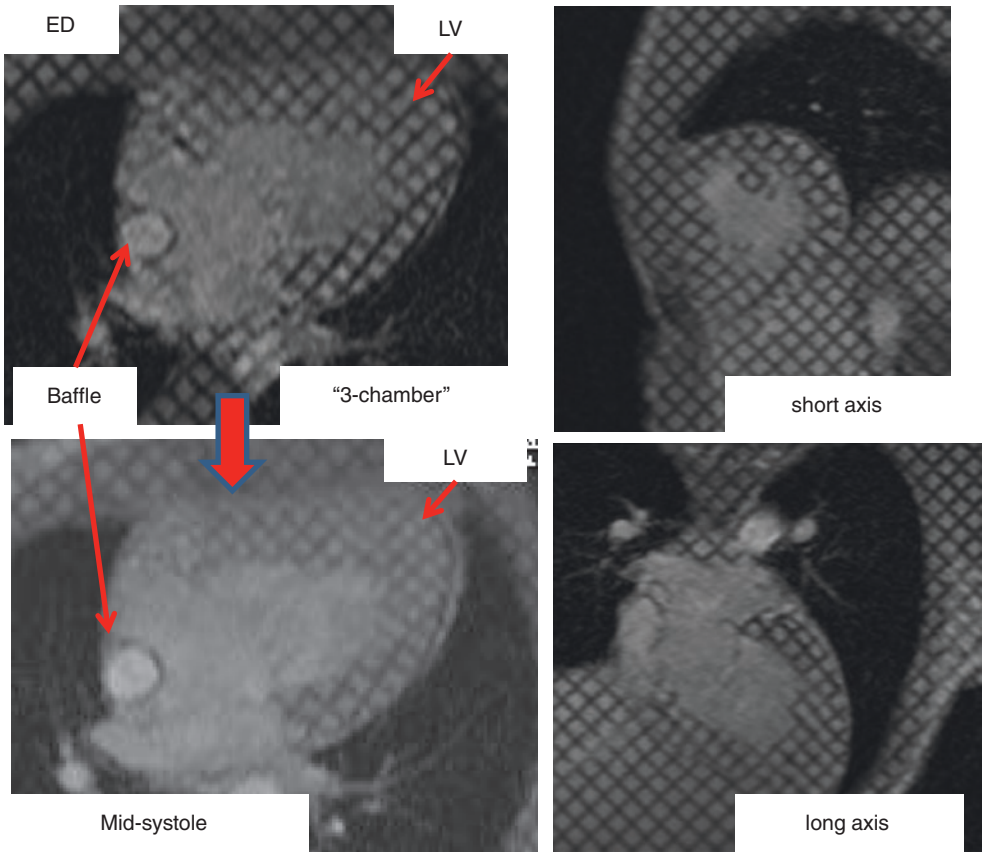

Fig. 1.11 Myocardial tagging in the "3-chamber" (upper and lower left), short axis (upper right), and long axis views (lower left) of a patient with a single left ventricle after Fontan. This is an example of spatial modulation of magnetization (SPAMM) where a grid is laid down on the myocardium and deformation can be visualized [6–9]. Note the deformation from end-diastole (ED, upper left) to mid-systole (lower left) in the "3-chamber" view. It is the equivalent of speckle tracking in echocardiography except by CMR; the "speckles" are purposefully created in a certain geometry for strain and wall motion assessment

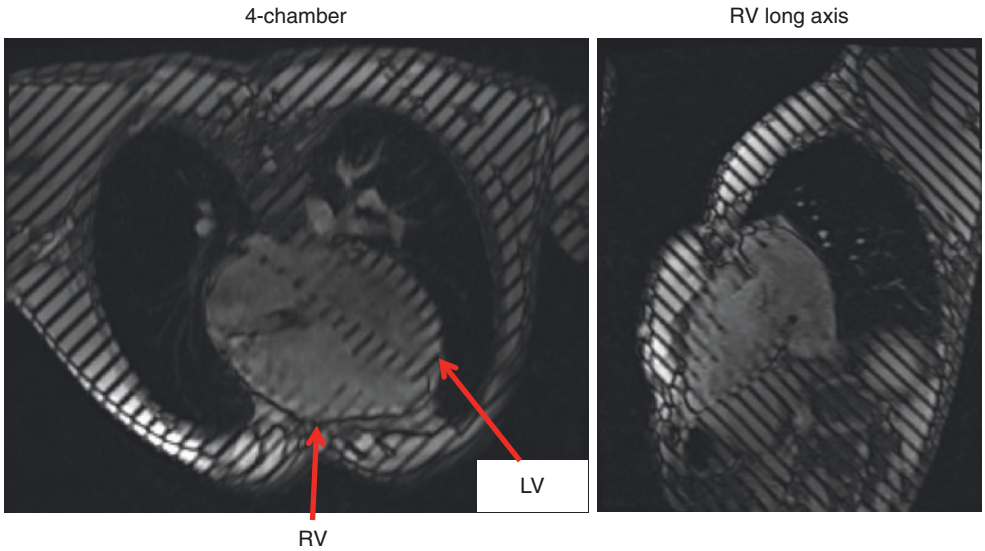

Fig. 1.12 Myocardial tagging in the "4-chamber" (left) and long axis of the right ventricle (right) in a patient with pulmonic stenosis after balloon dilation. Note how this differs from Fig. 1.11 with one set of parallel lines laid down on the myocardium—the so-called 1-dimensional tagging [10]

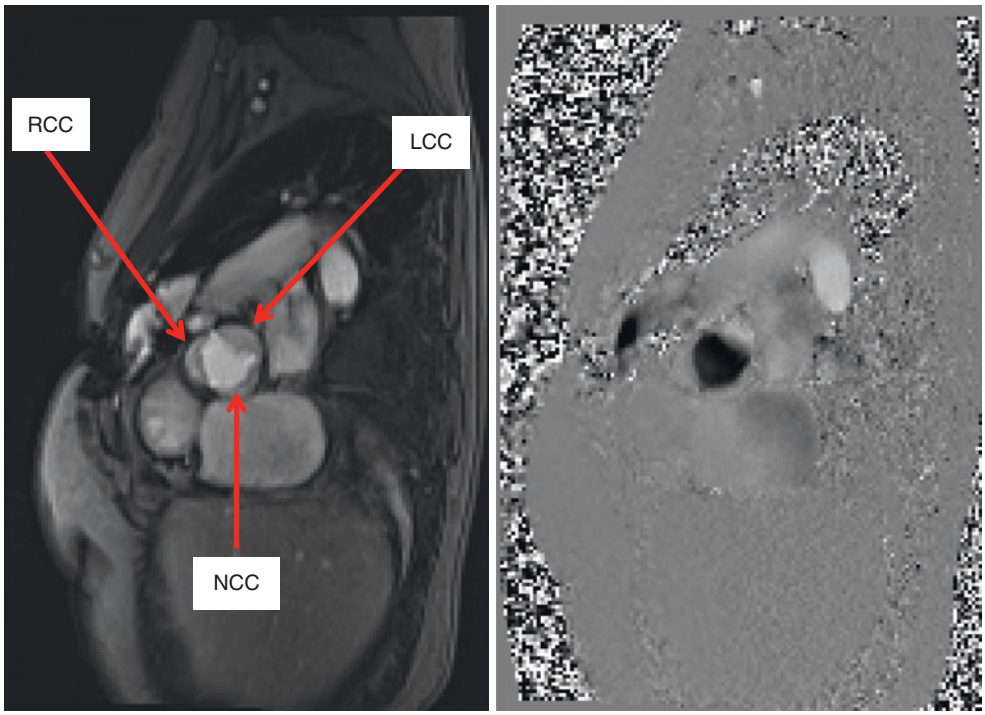

Fig. 1.13 Gradient echo imaging (left) and through plane phase-encoded velocity mapping (right) of the aortic valve. Note how the right (RCC), left (LCC), and non-coronary commissures are easily visualized on both images, demonstrating the trileaflet valve

the less lines of *k*-space per heartbeat (i.e., the number of segments inversely proportional to the time it takes to create the image). It is also true, however, that the more lines of *k*-space acquired per heartbeat, the worse the temporal resolution will be (i.e., the number of segments inversely proportional to the number of time points that can be created in the cardiac cycle). Tradeoffs are part of CMR and for most applications such as phase contrast velocity mapping and flow, image creation can be obtained in a breath-hold. It is important to realize that a regular cardiac rhythm is needed to ensure that lines of *k*-space from each cardiac cycle is acquired during the same point in time of the cardiac and respiratory cycles. In patients with arrhythmias or an inability to breath-hold, single-shot or real-time methods are commonly used [14] although there are also arrhythmia rejection techniques whereby an R-R interval and target heart rate are set and only beats falling within that range are accepted to build the image. For those patients who cannot hold their breath, using segmented techniques with multiple "averages" or "excitations" can be used to smooth out the respiratory motion at a minor cost to image fidelity (most times).

5. *Image Reconstruction:* As mentioned above, the Fourier transformation is used to create an image from the lines of *k*-space which is acquired from the MR signal. A technique called "partial Fourier" or "partial *k*-space" has been used for many years which reduces scan time with a lower signal-to-noise than using a "full" Fourier transformation. Parallel imaging with names such as SENSE [15], SMASH, GRAPPA, and TSENSE [16] uses multiple coils and multiple channels and has become ubiquitous in many sequences; they sample only a fraction of the full *k*-space but yet allow for a full field-of-view and resolution images with significant time savings at the cost of signal-to-noise. Compressed sensing CMR is another method that undersamples *k*-space losing very little fidelity to speed up the image acquisition and to reconstruct images that are nearly indistinguishable from those that do not undersample *k*-space [17].

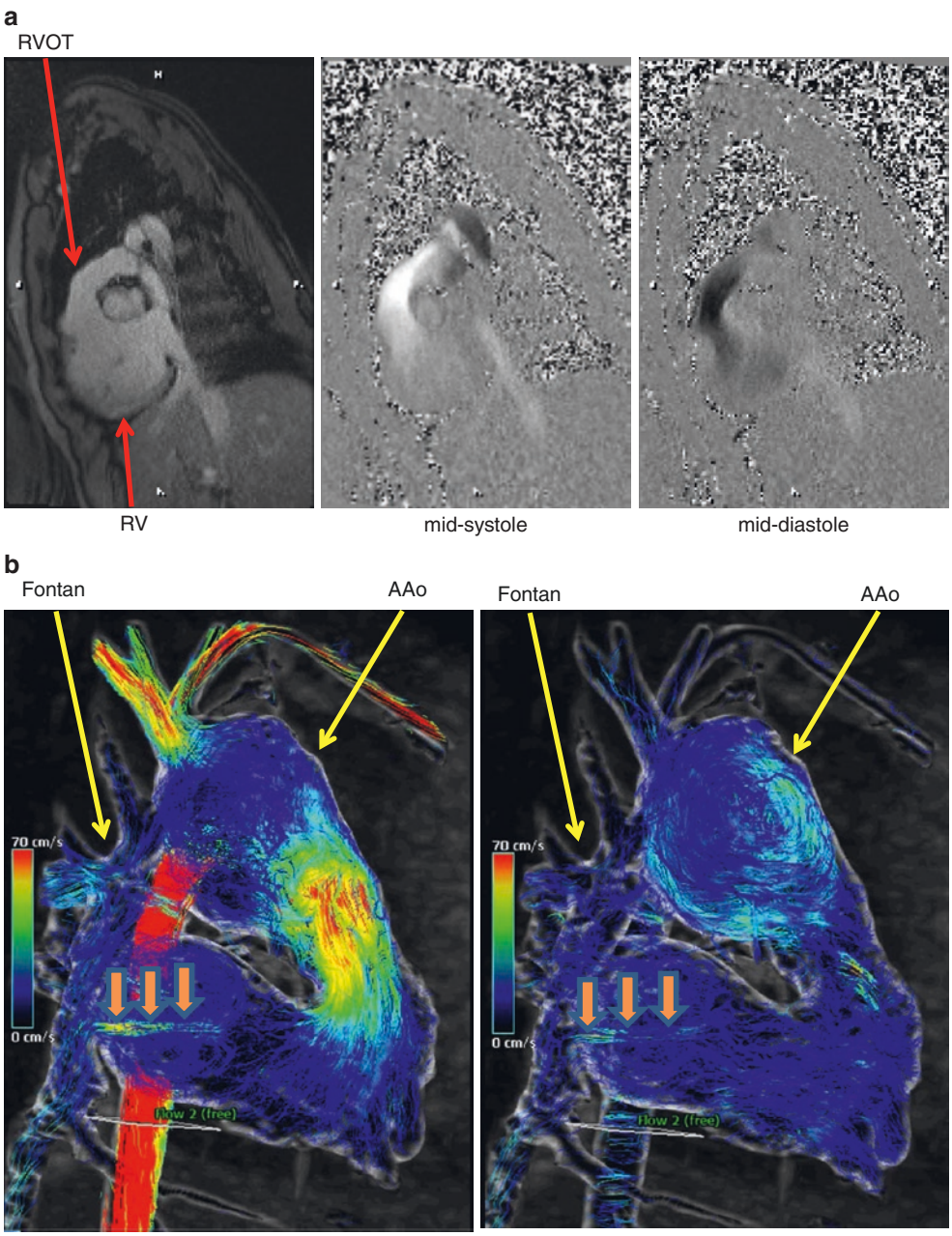

Fig. 1.14 (**a**) In-plane phase-encoded velocity mapping in a patient with double outlet right ventricle after a right ventricle to pulmonary artery conduit. On the left is a magnitude image of the right ventricular (RV) outflow tract (RVOT). In the middle is a mid-systole frame of the in-plane phase-encoded velocity map in the exact orientation and position as the image on the left where flow cephalad is signal intense; on the right is a mid-systolic frame where flow caudad is signal poor (dark on the image) indicating severe conduit insufficiency. (**b**) 4D flow in systole (right) and diastole (left) of a single ventricle patient after Fontan. Note the fenestration flow (arrows) and the vortex formation in the dilated ascending aorta (AAo)

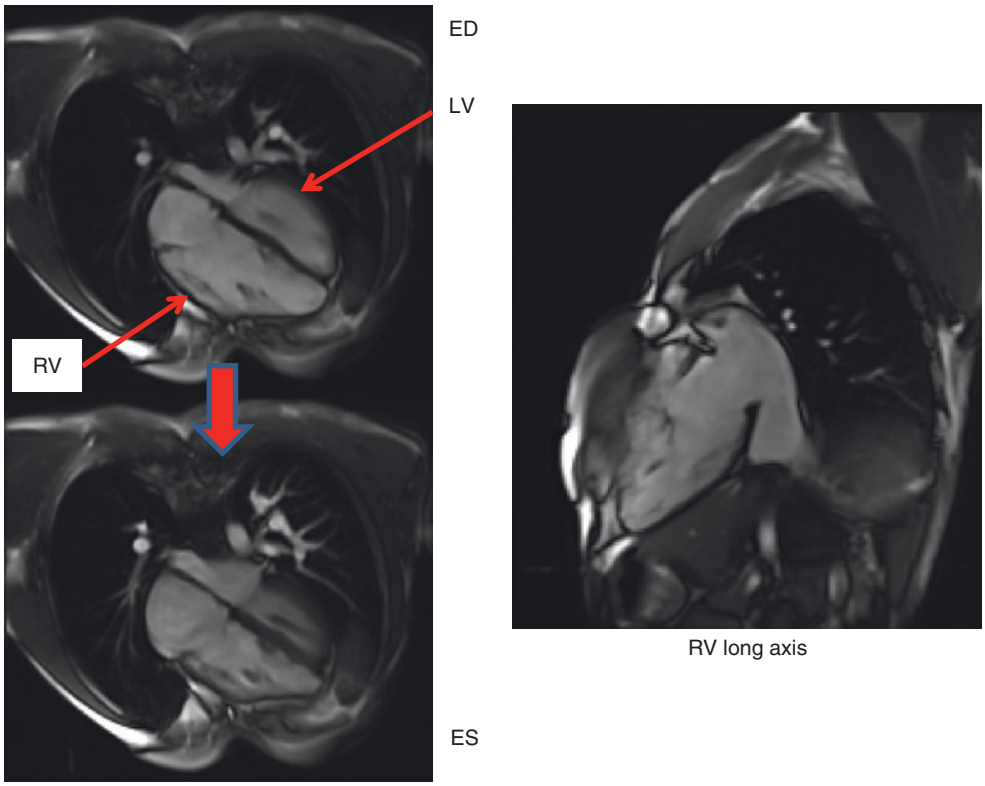

Fig. 1.15 Steady-state free precession imaging in the 4-chamber view (left) at end-diastole (ED, upper) and end-systole (ES, lower) in a patient with tetralogy of Fallot. The long axis of the right ventricle (RV) is on the right. *LV* left ventricle

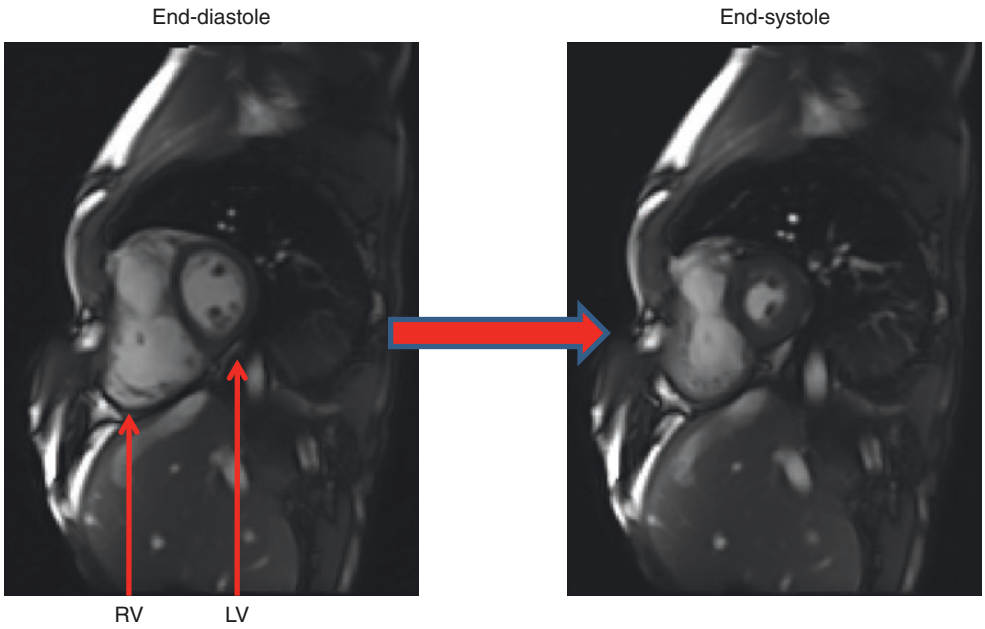

Fig. 1.16 Steady-state free precession imaging in the short axis view at end-diastole (ED, left) and end-systole (ES, right) in the patient with tetralogy of Fallot in Fig. 1.15

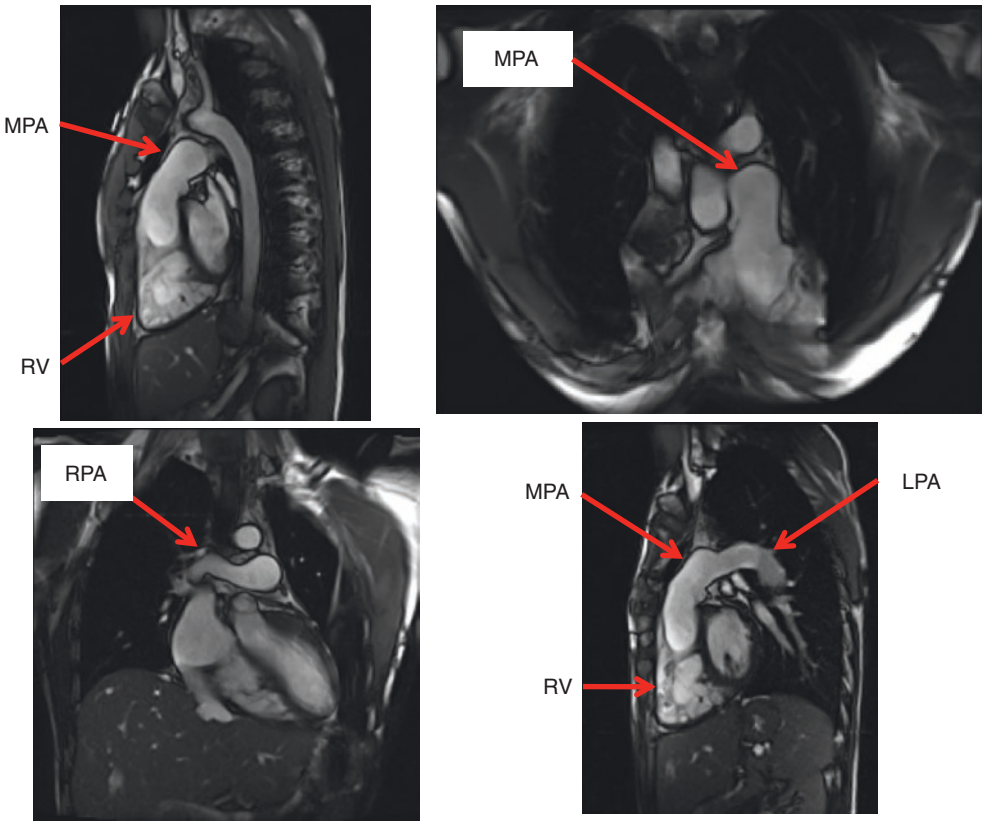

Fig. 1.17 Various steady-state free precession cines of the patient in Figs. 1.15 and 1.16 with tetralogy of Fallot. The right ventricular outflow tract views are seen in the upper panels in off-axis sagittal (left) and coronal (right) views which are orthogonal to each other. The right (RPA) and left pulmonary arteries (LPA) are seen in long axis in the left lower and right lower panels respectively. *MPA* main pulmonary artery, *RV* right ventricle

1.3 Prospective Triggering/Retrospective Gating

Because the heart needs to be at the same phase of the cardiac cycle with any segmented technique, as noted above, a way is needed to determine this phase. This is nearly universally the R-wave of the ECG. A static or non-moving image uses the R wave to signal the beginning of systole as is the touchstone of the cycle; the CMR sequence then begins. This technique is called prospective triggering since the sequence is initiated by the R wave; lines of *k*-space are then acquired. Phases of the cardiac cycle are defined by a fixed time after the R-wave, so small perturbations of rhythm will put the heart at a slightly different point in the cardiac cycle; this generally does not affect the image too much. In addition, there is generally some "dead space" prior to the next R wave so very late diastole is usually not imaged or utilized. Cine or moving images are acquired by either this method or the method of retrospective gating. With retrospective gating, lines of *k*-space are acquired continuously regardless of the phase of the cardiac cycle while the ECG is simultaneously recorded; after image acquisition, the software "bins" the lines of *k*-space relative to the ECG and cardiac cycle. In this way, each cardiac phase is defined as a certain percentage of the cardiac cycle, allowing the actual duration of each phase to vary flexibly with variation in cardiac cycle. In addition, no "dead space" is left prior to the next phase which can be important in assessing flows or ventricular function.

The above paragraph makes a distinction between static and dynamic techniques. Static ones are generally used for cardiovascular anatomy or characterizing tissue. Dynamic techniques are used to assess function or flow in addition to anatomy. A run of single-shot images, acquired quickly, can be strung together as motion and this is termed "real-time" and is asynchronous with the cardiac cycle; this can be used in cine imaging, phase contrast velocity mapping, or dynamic 3D angiography. First-pass perfusion imaging can be thought of as a hybrid between static and dynamic imaging, where each image depicts a different phase of the cardiac cycle over time.

1.4 ECG Signal

For many years, the upstroke of the R wave on the ECG signal was used to trigger the scanner and used as a marker for end-diastole; unfortunately, artifacts occurred because of the high magnetic field strength and radiofrequency pulses which precluded reliable detection of the true R wave. Bizarre T waves and spikes during the ST segment of the ECG would cause the triggering to falsely detect these waves as the R wave. This is especially true in congenital heart dis-

ease where abnormal QRS axes and bundle branch blocks from surgery can make the distinction of the R wave even more problematic in the scanner. On most systems in use today, detection of the R wave as a trigger has been replaced by the use of vectorcardiography (VCG), which is less susceptible to distortion from the magnetic field and of flowing blood in the thoracic aorta which can act as a conductor. Although wired connection between the VCG and the imaging systems has been utilized in the past, this has been nearly universally replaced by wireless transmission which allows for more flexibility in the scanner.

There are alternatives to the direct connection between the "MRI ECG" and the patient. The ECG signal from external monitoring systems such as the anesthesia equipment can be used which can generate a signal contemporaneous with the R-wave to the MR scanner. Alternatively, the ECG signal can be discarded for "peripheral pulse triggering" where a finger or ear pulse may also be used; obviously, this requires good peripheral circulation. If the patient is cold or has a coarctation, this will often be unsuccessful. It also should be noted that because there is a delay in transmission of the pulse to the distal part of the body that is being monitored, the waveform will be delayed by 200–300 ms when compared with the ECG; this needs to be taken into account during the analysis and interpretation phase of the examination. Peripheral pulse gating is especially useful in patients where a good detection of the R wave cannot be obtained otherwise. Another alternative is the use of non-triggered SSFP sequences where lines of *k*-space are continually being obtained by the imaging system without regard to the ECG or respiration (see above and below). With the use of parallel imaging in the spatial or time domains, a temporal resolution as high as 30–40 ms can be acquired; even higher temporal resolution can be obtained by combining this with compressed sensing. This type of imaging can be used in patients with arrhythmias to obtain functional information when triggering the ECG is problematic (see below). Finally, recent advances in hardware and software have enabled the use of "self-gating" sequences, where a coil is used to monitor the motion of the ventricle which is used as a signal for ventricular contraction and relaxation. This approach allows the heart itself to be monitored and act as its own signal for the imager; retrospective analysis of the lines of *k*-space can then be "binned" to construct moving images. There are now techniques that not only "self-gate" but also compensate for respiration where a 3D cine data set can be acquired at multiple respiratory phases without an ECG or navigator (see below) [18].

A special note is required on patients with arrhythmias. With frequent premature ventricular contractions, runs of supraventricular tachycardia or trigeminy for example, it is unclear what an ejection fraction, cardiac index, or end-diastolic volume would mean given that these ventricular performance parameters can change from beat-to-beat. A qualitative assessment using real-time steady-state free precession is one way to get a handle on ventricular function. Nevertheless, there may be instances when some quantitative information may be needed; in these particular cases, "arrhythmia rejection" can be used (see above). With this approach, a range of heart rates or R-R intervals can be set, and the imaging system will only allow those lines of *k*-space which meet these requirements into the final image; the rest of the lines of *k*-space which fall outside these heart rates are ignored. This approach is inefficient, however, in this manner, quantitative ventricular performance information can be obtained for a range of heart rates. For example, if the range is set between an RR of 700 and 800 ms, the resulting cardiac index can be said to be present for heart rates between 75 and 86 beats/min. Finally, some real-time cine sequences have arrhythmia compensation built in [14].

1.5 Respiration

Besides cardiac phases, respiration must be dealt with as it causes positional variation of the heart from movement of the lungs and diaphragm; if not taken into account, this will lead to motion artifacts. There are a number of ways in which this is dealt with in CMR:

1. Breath-holding, where the patient's breath is held during image acquisition. For many common applications such as cine and phase contrast velocity mapping, image acquisitions are fast enough to be performed in a reasonably short breath-hold. This can be done in adults or in children under anesthesia who are paralyzed, intubated, and mechanically ventilated. These pulse sequences are widely available and commonly used routinely.
2. Signal averaging, also termed multiple excitations, where the signal from the complete image is "averaged" over many respiratory and cardiac cycles, "averaging out" the respiratory motion and making the image sharper than without this technique but less sharp than breath-holding. This can be used in small children unable to voluntarily breath-hold or adults who cannot cooperate. It has the advantage of being more "physiologic" and representative of the true state of the patient's physiology as the patient is continually breathing the information is averaged over many respiratory cycles.
3. Respiratory gating, where the motion of the diaphragm or the chest wall is tracked by either a navigator pulse (which tracks diaphragmatic motion, the equivalent of an "M-mode" of the diaphragm on echocardiography), respiratory bellows which are placed around the chest wall, or a signal from the respirator if the patient is under anesthesia. Lines of *k*-space are continuously acquired

during the cardiac cycle and only those lines of *k*-space which fall within certain positional parameters of the diaphragm or chest wall are incorporated into the image; the others are discarded. Although this is a very inefficient method of imaging, it is very effective and used in imaging coronary arteries, for example, where high resolution is needed. Whole heart angiography is also unsuitable for anything but respiratory gating.

4. Single-shot imaging, where all the lines of *k*-space are acquired within a single heartbeat. Advances in hardware and parallel imaging have dramatically improved the speed and quality of these single-shot and real-time techniques and are now often used for scanning patients unable to breath-hold.
5. The newer "self-gated" techniques, referenced above, that also compensate for respiration where a 3D cine data set can be acquired at multiple respiratory phases without an ECG or navigator [18].

1.6 Contrast Agents

These agents offer another important source of distinguishing tissues from each other besides the intrinsic properties of T_1, T_2, and T_2* for example. The most commonly used imaging agents, the paramagnetic chelates of gadolinium (Gd^{3+}), generally work by predominantly shortening T_1 and to a certain extent T_2; they generally enhance the signal on T_1-weighted images. Gadolinium, which has a very large magnetic moment, has unpaired orbital electron spins and shortens T_1 by allowing free protons to become bound creating a hydration layer, which helps energy release from excited spins and accelerates the return to equilibrium magnetization. For other contrast agents which predominantly shorten T_2, the reverse is true; shortened T_2 leads to decreased signal on T_2-weighted images. The effects of these agents can be described by the following formulae:

$$\frac{1}{T_1} = \frac{1}{T_{1_0}} + r_1 C$$

$$\frac{1}{T_2} = \frac{1}{T_{2_0}} + r_2 C$$

where T_{1_0} and T_{2_0} are the relaxation times prior to and T_1 and T_2 are the relaxation times after contrast agent administration, C is the concentration of the agent, and r_1 and r_2 are the longitudinal and transverse "relaxivities" of the individual agent (which are field strength dependent). CMR applications which utilize these agents include delayed enhancement, first pass perfusion, coronary angiography in certain sequences, and characterization of tumors and masses.

Another contrast agent that has become increasingly used is ferumoxytol, which is an iron-based contrast agent that is administered slowly over 15 min. This contrast agent has the distinct advantage of having a long half-life in the blood so that high-resolution segmented imaging may occur. This contrast agent is generally used in conjunction with high-resolution static inversion recovery gradient echo imaging to visualize coronary arteries, to perform whole heart 3D imaging, or to enhance 4D flow imaging signal [19] (see below). In addition, ferumoxytol has been used to acquire 4D whole heart cine imaging to obtain a 3D beating heart [20], combining anatomy, cine imaging, and 4D flow [19] and for the self-gated technique mentioned above that acquires cine at multiple respiratory cycles [18] (see above).

The safety profile of these agents is beyond the scope of this chapter. However, it should be noted that there has been a recently published multicenter trial of ferumoxytol demonstrating a safety profile equivalent to other imaging agents and in certain regards, better [21].

1.7 Remaining Motionless in the CMR Scanner: Anesthesia and Sedation

The degree of cooperation necessary for successful performance of CMR is generally greater than that of any other type of MRI examination; scans require no significant movement, repeated breath-holds at the same point of the respiratory cycle over a period of 45 min to an hour, and can be lengthy. Couple this with the strange environment of the scanning room and the loud banging noises, it is no wonder that both adults and children alike find this very intimidating. Therefore, the use of medication may be required; either conscious sedation or general anesthesia is generally administered so that children who are too young to cooperate or adults with congenital heart disease who may not want to cooperate for one reason or another (e.g., claustrophobia) can still undergo successful CMR. With conscious sedation, patients continue to breathe throughout the scan and imaging has to be substantially altered because of this whereas in a paralyzed, intubated, and mechanically ventilated patient under general anesthesia, the effect of "breath-holding" can be created by having the anesthesiologist temporarily suspend ventilation. This is not to say that anytime a patient undergoes general anesthesia in the CMR environment that suspending respiration should be performed but rather that this technique is available to the CMR imager. It should be noted that imaging using sedation or general anesthesia with free breathing is much more physiologic than imaging with positive pressure mechanical ventilation and breath-holding (see above) and, therefore, may be more advantageous than the minor increase in image fidelity with breath-holding. For example, a single ventricle patient after Fontan depends

upon both cardiac and respiratory effects to allow for pulmonary blood flow; suspending respiration may alter the physiology artificially and therefore, although accurate for suspended respiration, the physiology is not reflective of the patient's true state. In addition, because systemic venous return changes during the respiratory cycle, imaging during suspended respiration will obtain data only in that state while if the patient is imaged during free breathing, the loading conditions across the respiratory cycle is "averaged" into the image and is more reflective of the patient's true physiologic state.

There is no definitive cut-off age for the age range where medication is needed to remain motionless for a successful CMR study; however, in general, most children greater than or equal to 10–12 years old can cooperate. Of course, this is just a rule of thumb as there can be 7-year-olds who are very mature and can follow directions while there are some 15-year-olds who will simply not cooperate and will require pharmacology. Limited scans with reduced times may be possible with younger patients who would normally require conscious sedation or general anesthesia and this may be considered; it is all in the judgment and purview of the family, physicians, and other healthcare providers caring for the patient. Preparation of the child prior to the scan is important; the involvement of child life experts, a supportive parent or other regular caregiver in the scanner room can reduce anxiety and be the difference between a scan under medication, without medication, or a successful versus an unsuccessful scan.

As the CMR environment can be a challenging one for the anesthesiologist or the pediatrician/nurse sedation specialist, monitoring is extremely important since the patient's body will be mostly within the scanner itself; direct visualization during the study is not possible without removing the patient from the bore of the magnet and removing the coil. Many centers utilize a direct video feed with cameras designed to work within the CMR environment and placed in critical positions. For example, a camera pointed down the bore of the magnet is essential along with cameras in other areas to get a good view of what is occurring in the scan room. In addition, extensive physiological monitoring of subjects using equipment specifically designed to be operated in the MR scan room is essential for the safe conduct of the study. Pulse oximetry, limb-lead ECG, blood pressure monitoring, inspiratory and expiratory gas analysis such as end-tidal carbon dioxide, and temperature monitoring (especially in young children) should all be available and used. The monitoring systems should be available wherever the anesthesiology/sedation teams are positioned; this is generally either in the control room or scan rooms. Many facilities position the anesthetic equipment and gas tanks directly outside the scan room, with the gas lines passing through "wave guides" in the wall of the scanner room installed for just this purpose. This arrangement has two advantages: (a) there is reduced risk of inadvertently introducing non-CMR compatible equipment into the scan room and (b) communication between the anesthesiology/sedation team and imaging teams is much easier in this setup. It should be noted, however, that this comes at the cost of increased compliance in the anesthetic circuit. If the decision is made to keep monitoring and anesthetic equipment in the scan room, there is usually a minimum distance that this equipment must be kept from the magnet within which it may not operate correctly, may interfere with the images, and might even be attracted into the scanner bore. Careful establishment of this distance from the manufacturer is mandatory before the equipment is first introduced into the scan room. Even the use of physical restraints to prevent incursion of the equipment within such a distance, and thus avoid accidents, should be considered. Direct verbal communication between the anesthesiology/sedation teams and the imaging teams should be on-going at all times with visual contact preferably as well.

Neonates and very small infants less than 6 months of age may undergo CMR successfully while sleeping using a "feed and swaddle" technique [22, 23]. The patient usually is kept awake for a while prior to scanning (3–4 h); when the child enters the preparation area, the intravenous is inserted and the ECG leads are placed. At this point, the baby is very fussy; however, feeding the infant and subsequently swaddling with a warm blanket in a quiet and dimly-lit environment prior to the study will allow the patient to fall asleep; the patient is subsequently transported to the scanner room. Vacuum-shaped support bags can also be utilized to reduce patient motion; placing ear plugs, a hat over the head and ears as well as blankets around the head all aid in keeping the child comfortable and asleep. Imaging sequences that allow for free breathing must be used.

Whether to use deep sedation or anesthesia to perform CMR has been debated for many years. Consideration should be given to how long the CMR scan is likely to take, the patient's age, the flexibility of CMR scanner time, and the availability of anesthesiology staffing and/or the availability of specialized sedation teams which include nurses and pediatricians. The practice is obviously a matter for individual, institutional, and patient preferences. Anesthesia is much more predictable when it comes to onset of action and duration/depth of impaired consciousness; this is advantageous in scheduling CMR examinations and running the schedule smoothly. Deep sedation use has been associated with reduced image quality in some studies [24] but not in others [25], and in some institutions, is far more likely to fail than anesthesia [26], though failure rates can be reduced to close to zero [25] by careful use of expert personnel and strict sedation regimes [25, 27–30]. Imaging performed under anesthesia can be shorter "in theory" because of the

ability to breath-hold; in practice, however, the scanning time difference is marginal at best and breath-holding, as mentioned above, is less physiologic. Anesthesia has been reported to be marginally safer than deep sedation in some studies [24, 31] and equal in others [25], but there is no doubt that it is more costly and invasive. There are numerous pediatric centers with many years of experience at performing CMR under deep sedation with excellent safety records [25, 27, 28, 30]. The end result is that both techniques are likely to remain in practice for the foreseeable future.

1.8 The Standard Pediatric/Congenital Heart Disease Examination

There are numerous protocols for a standard CMR examination of the heart, many equally as valid as the other. The one presented in this chapter is meant to be as complete and as efficient as possible; however, it should be recognized that this is not the only one. As each phase of the protocol is delineated, the technique utilized will be expanded upon in detail to give the basics of the different types of CMR.

1.8.1 Axial Imaging (Fig. 1.18)

The initial part of the examination begins with a set of static steady-state free precession (bright blood) images in the axial (transverse plane) extending from the thoracic inlet to the diaphragm. Generally, 45–50 contiguous end-diastolic slices are obtained of three (for babies) to 5 mm in thickness; end-diastole is acquired by placing a "delay" after the R wave of the ECG. At this point in the cardiac cycle, the heart is relatively motionless, allowing for high-fidelity imaging. This set of data, which usually takes two and a half to four and a half minutes to acquire (depending upon the patient's heart rate and size), is utilized as a general survey of the anatomy and may be used as a localizer for subsequent higher fidelity cine imaging, flow measurements, etc. These images are usually acquired with multiple averages (generally 3) during free breathing. In babies, to maintain signal to noise but nevertheless obtain thinner slices, overlapping slices can be used; the cost is prolonged acquisition time.

1. From this survey, a number of features may be gleaned with regard to cardiovascular structure in congenital heart disease [32]: (1) the position of the heart in the chest and

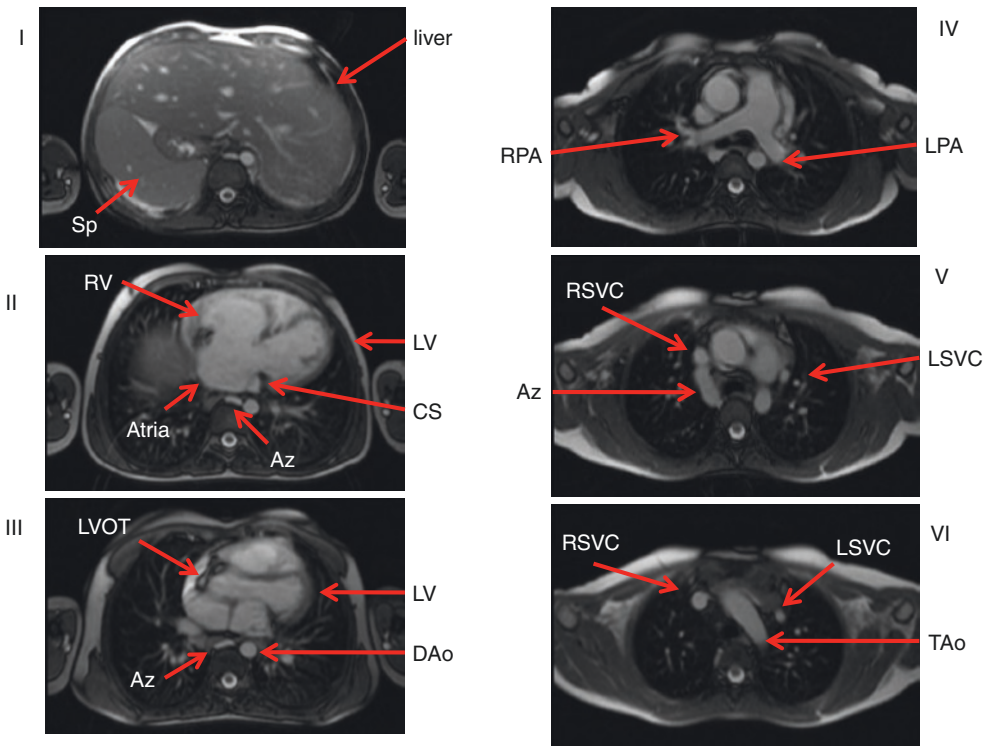

Fig. 1.18 Selected initial axial images of a patient with heterotaxy and complete common atrioventricular canal. Note how much can be gleaned from the first set of static steady-state free precession images. Images progress from inferior to superior as the roman numerals increase from top to bottom and from left to right. In I, a transverse abdominal view shows a midline liver and spleen (sp) on the right. In II, note the complete common atrioventricular canal, the dilated coronary sinus (CS), and dilated mildline azygous (Az). In III, note the widely patent left ventricular outflow tract. IV (top right) demonstrates the main pulmonary artery as well as the right (RPA) and left pulmonary artery (LPA) being confluent. In V, note how the dilated AZ enters the right superior vena cava (RSVC) as well as the presence of a left superior vena cava (LSVC). Finally, in VI, note the left aortic arch along with the RSVC and LSVC without a bridging vein. *TAo* transverse aortic arch

in which direction the apex is pointing, (2) normal cardiac segments (atria/ventricles/great arteries), (3) the intersegmental connections (atrio-ventricular and ventriculo-arterial), (4) veno-atrial connections, (5) aortic arch anatomy such as coarctation of the aorta and sidedness of the aortic arch, (6) pulmonary arterial tree (such as pulmonary stenosis, pulmonary sling), (7) extracardiac anatomy and its relationship with the cardiovascular system such as the trachea and tracheobronchial tree, abdominal situs such as the position of the liver, spleen, and stomach, qualitative assessment of lung size (e.g., important in Scimitar syndrome). For lesions such as main and branch pulmonary artery stenosis and coarctation of the aorta, off-axis imaging planes are necessary to confirm and better display these findings; however, these lesions can often be inferred from the stack of axial images. Qualitative assessment of lung hypoplasia and unbalanced pulmonary blood flow can be roughly estimated by the pulmonary vascular markings. If the study is ordered to determine if the patient has a vascular ring, the diagnosis is nearly always readily obtained using this stack of images using the feed and swaddle technique if an infant mentioned above [23]. Image acquisition time for the three-dimensional dataset can be accomplished in 20–30 s depending on the patient's heart rate.

2. There are drawbacks to using the axial stack when using it for diagnostic purposes; it must be remembered that is solely a survey and to be used as localizers for higher resolution imaging. As examples, smaller anatomic structures such as the pulmonary veins may not be visualized well or seem to appear to be connected anomalously but really be connected normally because of partial volume effects. Follow-up with off-axis imaging is mandatory.
3. In addition to the axial stack of SSFP images, a set of HASTE (Half-Fourier-Acquired Single-Shot Turbo Spin Echo) axial images (Fig. 1.19) can be very useful and are usually obtained while multiplanar reconstruction is being performed on the SSFP images (see below). HASTE is a dark blood, single-shot (image obtained in one heartbeat) technique which is low resolution and acquired during free breathing, generally obtained in 1–2 min. If the RR interval of the patient is under 600 ms, the images are generally acquired every other heartbeat (doubling the acquisition time) to allow the protons to relax further. HASTE images are less susceptible to flow artifacts and metal artifacts. For example, turbulence in the systemic to pulmonary artery shunt (Blalock-Taussig shunt) or Sano shunt in a single ventricle patient after Stage I Norwood reconstruction will demonstrate signal loss in the shunt itself and the pulmonary arteries on SSFP imaging. Turbulent flow occurs in diastole as well as systole in this scenario and recalling that the static SSFP images are acquired in diastole, these structures are difficult if not impossible to see on the SSFP images. These structures are, however, readily visualized on the HASTE images. Multiple patients can present with braces on their teeth which is common in adolescents as well as stents in their great arteries or other blood vessels; these metallic objects can and generally do produce artifacts which appear on the SSFP imaging, but not on the HASTE images. Note, however, that because of the "cage effect" (see below in the dark blood section 1.8.3), direct measurement of the cavity of the stent is not possible. HASTE imaging can also be useful with visualizing regions of the coronaries and in characterizing masses; however, dedicated subsequent imaging of these structures is mandatory. The HASTE images give the imager a "first pass" at the problem and, similar to the stack of SSFP imaging, is simply a survey.

1.8.2 Multiplanar Reconstruction

During the acquisition of the HASTE images, multiplanar reconstruction is performed on the axial SSFP (or HASTE) images. Multiplanar reconstruction is the act of taking the contiguous stack of images and reconstructing these images into other planes (e.g., axial images being resliced as coronal images or in a double oblique angle to obtain the "candy cane" view of the aorta). Nearly all scanners today come with software which allows this to be readily performed. The purpose of this obviously is to obtain orientation and slice positions for dedicated images of the anatomy in question, functional imaging, tissue characterization, and blood flow. Further anatomy can be obtained with cine, the various types of dark blood imaging, or 3-dimensional contrast-enhanced images (see below). For the 3-dimensional contrast-enhanced slab, these axial images act to ensure that the anatomy in question is covered by the slab. Ventricular function and blood flow are obtained using cine and phase contrast magnetic resonance (PCMR) (see below). Off-axis imaging planes can be used, for example, to profile the ventricular outflow tracts, the atrio-ventricular valves, major systemic and pulmonary arteries and veins and all their connections to the heart.

1.8.3 Dark Blood Imaging (Figs. 1.8 and 1.20)

High-resolution dark blood imaging (as compared to the low-resolution HASTE images) is static in nature and is used sparingly because it is time consuming; 1–2 images can be obtained in a breath-hold. There are numerous types of dark blood imaging such as T_1 weighting, T_2 weighting, spin echo imaging, turbo spin echo imaging, double or triple inversion recovery, etc. This technique is generally utilized for tissue

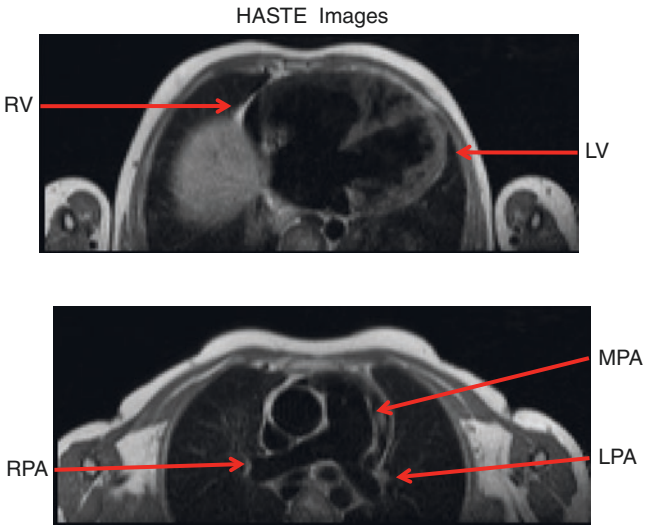

Fig. 1.19 Two initial axial HASTE images of the patient in Fig. 1.18 with heterotaxy and complete common atrioventricular canal. The upper and lower panels are equivalent to panel II and IV in Fig. 1.18; compare these images with those of Fig. 1.18

characterization and to define anatomy when turbulence or artifacts get in the way of bright blood techniques. The blood from the heart cavities and blood vessels is black while soft tissue is signal intense. Most dark blood imaging in children utilizes either T_1- or T_2-weighted imaging with the double inversion approach. The details of how each type of dark blood imaging is created are beyond the scope of this chapter; however, a simple example is instructive. The double inversion T_1-weighted dark blood technique is utilized to maximally suppress signal from blood and begins with a nonselective inversion pulse which can be thought of as flipping all the protons 180° throughout the body, destroying all the signal from these spins. This is subsequently followed by a selective inversion pulse which flips the protons once again 180° but in a selected region of the body (such as the imaging plane needed); a standard T_1-weighted spin echo sequence is then run. In this way, all the blood entering the imaging plane is signal poor with the spins destroyed in the nonselective inversion pulse and detailed endocardial or endovascular surfaces can be visualized. Dark blood imaging can be used,

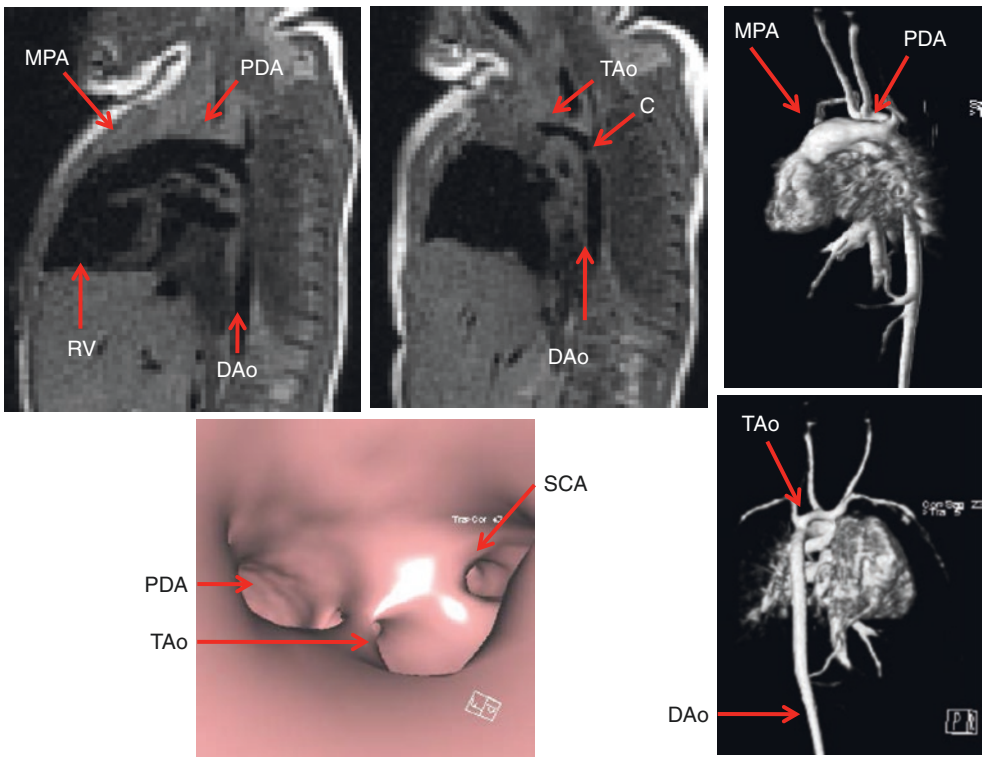

Fig. 1.20 Dark blood, 3-dimensional gadolinium and "fly-through" imaging of a neonate with hypoplastic left heart syndrome who has not undergone surgery. The left upper image is an off-axis sagittal view demonstrating the right ventricular outflow tract giving rise to the main pulmonary artery (MPA), patent ductus arteriosus (PDA) connecting to the descending aorta (DAo). The upper middle is similar to the upper left except a few millimeters over to the right demonstrating the hypoplastic transverse aortic arch (TAo), the coarctation (C), and the DAo. The right upper and right lower images are 3-dimensional reconstructions from a time-resolved gadolinium sequence which demonstrates the MPA, PDA, hypoplastic TAo and DAo from a sagittal (top) and posterior (bottom) view. The lower left is a "fly-through" image of the 3-dimensional reconstruction looking up from the DAo towards the os of the PDA, hypoplastic TAo and subclavian artery (SCA)

as mentioned above, to characterize different types of tissue as these will generate different signals. As an example, fat will be intensely bright on T_1-weighted imaging while myocardium will be much less so. In addition, special pulses can be used to change the signal intensity and determine if indeed this tissue is what is suggested; taking for example fat as was just mentioned, a "fat saturation" pulse may be coupled with dark blood imaging and will turn the very bright signal of fat without this fat saturation pulse into a very dark signal with the fat saturation pulse, confirming that the bright signal is indeed fat. This may be useful for lipomas—visualizing this mass on T_1-weighted images with and without a fat saturation can confirm the diagnosis. Triple inversion recovery may be used to delineate edema in the tissue from, for example, a myocardial infarction or myocarditis.

Typically, in our imaging protocols, if needed, this is performed after the SSFP and HASTE imaging but should not be used after gadolinium administration except for specific applications such as myocarditis or tumor characterization. If used after gadolinium administration, the blood pool will demonstrate signal which is counterproductive to the intent of dark blood imaging in the first place. Use for dark blood imaging besides myocarditis is to visualize the pericardium, image the tracheobronchial tree (useful in a vascular ring study), and tumor characterization (with and without gadolinium). As mentioned above, it is useful to image patients when coils, stents, braces, spinal rods, and other foreign material cause artifacts on bright blood imaging. Precise measurements cannot be performed within a stent, however, because of the "cage effect." The image artifact caused by the stent prevents the physician from seeing the critical area in and around the stent. This is caused by the fact that a metallic stent behaves as a "Faraday Cage" due to its geometry and material, and the stent additionally creates a magnetic susceptibility artifact due to the material of manufacture of the stent.

A more modern approach is the use of a 3D dark blood acquisitions such as SPACE (Sampling Perfection with Application-optimized Contrasts using different flip angle Evolution) which is not only gated to the cardiac cycle but also employs a navigator pulse to obtain high-resolution (1–1.2 mm isotropic) imaging. It is generally performed in systole, aiding to null the signal from blood. It has found utility in patients who have hardware in place such as stents or devices or where turbulence makes SSFP imaging problematic.

1.8.4 Cine (Figs. 1.10, 1.13, 1.15, 1.16, and 1.17)

Myocardial motion and blood flow can be visualized with cine imaging to determine function and physiology. It is one of the two workhorses of CMR in this regard (the other being phase contrast velocity mapping which will be discussed next). The two major types of cine imaging are unbalanced gradient echo imaging and SSFP as mentioned above. The unbalanced gradient echo technique is older but still has a number of uses in state-of-the-art CMR. For example, unbalanced gradient echo imaging is useful to determine valve morphology using a high flip angle (Fig. 1.13); in this way, flowing blood into the imaging plane is bright and outlines the leaflets of the valve very well. It is also useful when artifacts plague SSFP as a low echo time (TE) and high bandwidth gradient echo image is less susceptible to these artifacts. High TE gradient echo imaging will enhance turbulence (where SSFP is less susceptible to turbulence) and may be useful in identifying these areas of flow disturbances. It is also the cine workhorse when ferumoxytol is administered as the contrast agent, using a high bandwidth.

High-resolution SSFP cine imaging (Figs. 1.15, 1.16, and 1.17) can demonstrate exquisite images of the myocardium, valves, blood pool, and vessels. In assessing myocardial function, it is the technique of choice and the gold standard. These cine images provide excellent spatial and temporal resolution for the assessment of global and regional myocardial wall motion. These cine sequences should be retrospectively gated so that wall motion data is available for the entire cardiac cycle. As mentioned, with prospective triggering, the phases prior to the R wave is generally truncated as noted above in the physics section. With retrospective gating, the number of calculated phases should be figured so that there is only one or less interpolated phase between each measured phase; an interpolated phase is one that shares data between the two measured phases. This is easily performed by doubling the patient's RR interval and then dividing by the heartbeat "TR" (line TR × number of segments) to get the maximum number of phases or dividing by the number of phases desired to obtain the maximum TR needed.

Temporal resolution should be set to provide, in general, 20–30 phases across the cardiac cycle, depending upon the heart rate. Obviously, in a patient with a heart rate of 150 beats/min (R-R of 400 ms), 20 frames/heartbeat is more than adequate (20 ms temporal resolution) while if the heart rate is 50 beats/min (R-R of 1200 ms), 20 frames/heartbeat is not sufficient (60 ms temporal resolution). This is because systole does not vary too much as a function of heart rate; it is diastole that lengthens or shortens. A 60 ms temporal resolution for a heart rate of 50 beats/min will not capture enough frames in systole to adequately assess the ventricle.

When an entire ventricular volume dataset is acquired, ventricular volume and mass at end-diastole and end-systole are measured yielding end-diastolic and end-systolic volumes, stroke volume, ejection fraction, cardiac output, and mass [33–37]. To perform an entire ventricular volume set, generally a 4-chamber view is first obtained by cine (orientation and slice position determined by multiplanar reconstruc-

tion as noted above); the 4-chamber view is defined as the view that intersects the middle of both atrioventricular valves at the atrioventricular valve plane and the apex of the heart. Subsequently, a series of short axis views are obtained which are perpendicular to the 4-chamber view and span from atrioventricular valve to apex. It should be noted that this requires obtaining short axis slices one slice past the atrioventricular valve level and one slice past the apex to ensure the entire volume is obtained; this can be clearly positioned off the 4-chamber view at end-diastole. Measurement of ventricular volumes involves contouring the endocardial border of each slice of a given phase (e.g., end-diastole or end-systole) from base to apex and planimeterizing this area. The product of the sum of the areas on each slice encompassing the ventricle and the slice thickness yields the ventricular volume at that phase. This procedure, if performed at end-diastole and end-systole, will yield two values and the difference between these values is the stroke volume; and the ratio of the stroke volume to the end-diastolic volume multiplied by 100 yields the ejection fraction. The cardiac output is obtained by multiplying the ventricular stroke volume and the average heart rate during the cine acquisition (note that if there is atrioventricular valve insufficiency, a ventricular septal defect or there is double outlet ventricle, this will not equate to aortic outflow). Ventricular mass is similarly measured, generally at end-diastole, by contouring the epicardial border on each slice which contains ventricle and planimeterizing the area which contains both the ventricular volume and mass. This value is subtracted from the ventricular volume measurement at each slice and yields the ventricular mass multiplied by the density of the myocardium. Most scanners come with and numerous independent companies sell software which semiautomates this process; ventricular volumes and mass can generally be obtained in a few minutes of post-processing. More tedious is contouring ventricular volumes through every phase of the cardiac cycle; however, this will yield a ventricular volume–time curve which may be useful in some situations. Because CMR can acquire multiple contiguous, parallel tomographic slices, there is no need for geometric assumptions, making the technique an excellent tool for precise measurement of ventricular volumes and mass in congenital heart disease. Indeed, cine CMR is considered the "gold standard" for ventricular volume and mass in both adult cardiology, pediatric CMR, and congenital heart disease. Ventricular size and shape can vary considerably in various forms of congenital heart disease (e.g., single ventricles, corrected transposition of the great arteries, etc.). Ventricular cine is also utilized not only for global but for regional wall motion abnormalities as well.

Besides ventricular size, mass, and wall motion, cine imaging is excellent for identifying vessel sizes as well as stenosis or hypoplasia including great arteries, along a ventricular outflow tract or in a baffle or conduit. On the flip side, cine can also be used to qualitatively assess regurgitation of valves of which there should be minimal in the normal heart. All this is determined not only by the shape of the vessel but by loss of signal due to acceleration of flow through a stenotic vessel/valve or a regurgitant valve; a classic example is the flow void through coarctation of the aorta. In addition, shunts can be identified by cine as turbulence visualized across atrial or ventricular septae will indicate interatrial and interventricular communication. A way in which shunting can be accentuated visually is with the use of a presaturation tag. When the protons in a plane of tissue are flipped 180° to destroy their spins prior to imaging (similar to a selective inversion pulse in a plane of tissue intersecting the imaging plane), a presaturation tag is said to be laid down. This presaturation tag labels the tissue it intersects with decreased signal intensity (black on the image). If the presaturation tag is laid down on the left atrium prior to a gradient echo sequence in a patient with an atrial septal defect, blood flowing from left to right will be dark on the bright blood cine and visualized to cross from left to right atria. Similarly, if there is right to left flow, bright signal from the right atrium would be seen to cross to the darkness of the left atrium.

By stringing a series of continuous single-shot images together in one plane ("single plane, multiphase" imaging), motion can be captured and this is termed "real-time cine CMR" (see above). Essentially, the SSFP technique is used to acquire all the lines of *k*-space needed to create an image continuously in the same plane. "Interactive real-time cine CMR" adds the ability to be able to manipulate the real-time imaging plane interactively, similar to echocardiographic ("sweeps"); this provides a fast way to assess cardiovascular anatomy, function, and flow. These images can be used for localization for higher resolution regular cine CMR and have been utilized in the past to actually acquire fetal cardiac motion. It is also used in the event there is too much arrhythmia so that at least a qualitative assessment of the heart can be made. Temporal resolution can be as low as 35 ms using parallel imaging.

CMR techniques in general and cine in particular build the image of multiple heartbeats. If multiple averages (excitations) are used, this can be in the hundreds. The disadvantage to this is the time it takes to acquire the data unlike "real-time" CMR cine imaging just mentioned or echocardiography where the cardiac motion is instantaneously obtained. The distinct advantage to this approach, however, is because the image is built over many heartbeats; it represents the "average" of all those heartbeats over the acquisition time. This truly is an advantage as it would be assumed that this "average," embedded in the image, is more reflective of the patient's true physiologic state than the instantaneous images of echocardiography. To perform the equivalent, the echocardiographer would have to view hun-

dreds of heartbeats and "average" it in the imager's mind with all the subjectivity that entails. Picture measuring hundreds of M-mode dimensions of the ventricle (end-diastolic and end-systolic diameters) and then averaging them all together to get a shortening fraction: that is what is obtained with cine CMR in one image when measuring ventricular function parameters!

1.8.5 Phase Contrast (Encoded) Magnetic Resonance (PCMR) (Figs. 1.13, 1.14, 1.21, 1.22, and 1.23) [38–46]

This CMR technique, also known as "velocity mapping," is used to measure flow and velocity in any blood vessel with few limitations (for example, generally 4–6 pixels must fit across the blood vessel in cross-section for it to be accurate). Broadly speaking, there are two types of PCMR—through plane which encodes velocity into and out of the imaging plane and in plane which encodes velocity in the imaging plane (as in Doppler echocardiography). For example, through plane PCMR can measure cardiac output, the aortic, and the pulmonary valves by measuring the velocities across the valves in cross-section, multiplying by the pixel size summed across the entire vessel, integrated over the entire cardiac cycle, and multiplied again by the heart rate. In the absence of intracardiac shunts, the flows across the aortic and pulmonary valves should be equal—an internal check to the measurement. In another example, relative flows to each lung may be measured by utilizing through-plane velocity maps across the cross-section of the right and left pulmonary arteries, obviating the need for nuclear medicine scans. By placing a through-plane velocity map across the main pulmonary artery, an internal check on the branch pulmonary artery flows is obtained as the sum of the blood flow to the branch pulmonary arteries must equal the blood flow in the main pulmonary artery. In addition, it is also common to utilize PCMR as a check on cine measurements (e.g., cardiac index of the aorta should be equal to the cardiac index of the left ventricle in the absence of mitral insufficiency or intracardiac shunts). It is clear that this is a strength of CMR—the ability to perform these checks for internal validation of the quantitative data, unlike other imaging modalities.

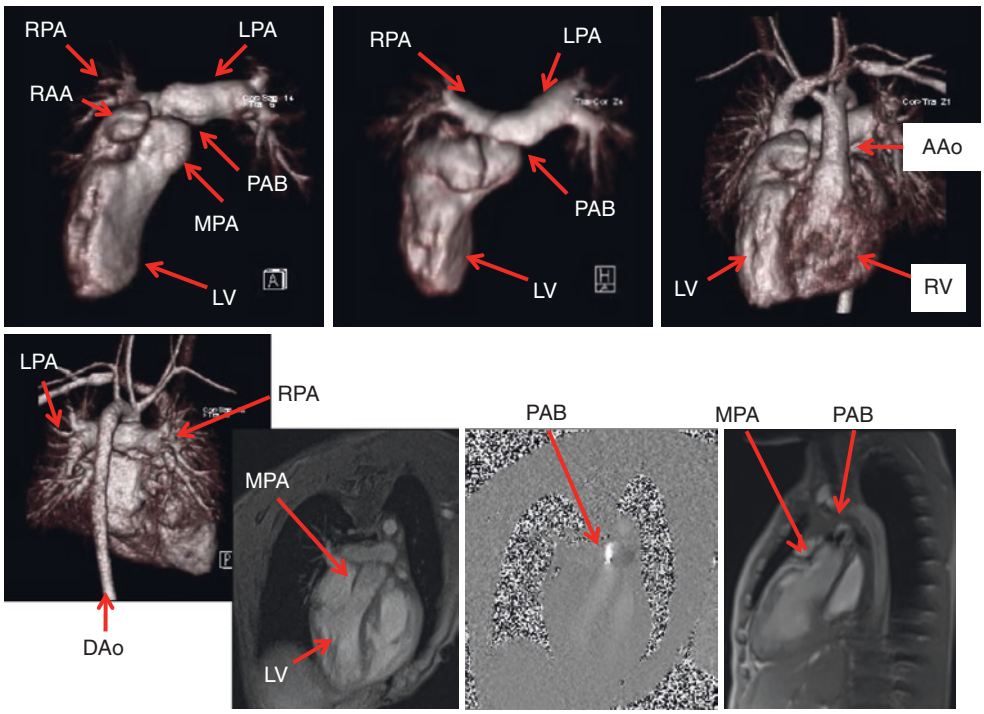

Fig. 1.21 Various types of imaging in an infant with corrected transposition of the great arteries after a pulmonary artery band (PAB). The upper left and middle panels are two views of a 3-dimensional gadolinium image of the right-sided circulation showing the left ventricle, main pulmonary artery (MPA), PAB, and the right (RPA) and left pulmonary arteries (LPA) from anterior (left) and anterior tipped up to transverse view (middle). Note how the right atrial appendage (RAA) is easily seen. The right upper and left lower images are 3-dimensional gadolinium reconstructions of both circulations demonstrating the anterior aorta and branch pulmonary arteries form the anterior (upper right) and posterior (lower left) views. The lower panel second from the left and second from the right are magnitude and in-plane phase images from phase-encoded velocity mapping demonstrating the left ventricular outflow tract and showing the jet through the PAB (signal intense is caudad) with a VENC of 400 cm/s. The right lower image is an orthogonal view through the left ventricular outflow tract demonstrating the turbulence distal to the PAB

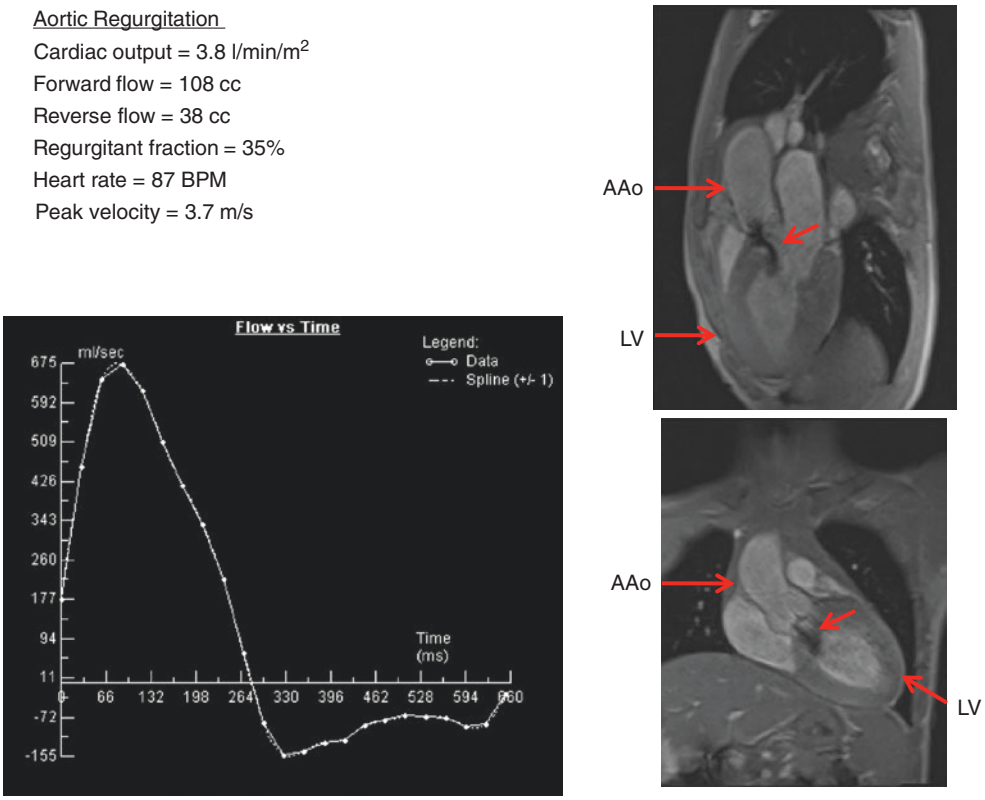

Fig. 1.22 Data and images from a patient with a bicuspid aortic valve, aortic stenosis, and insufficiency. The graph of flow versus time is on the lower left and on the upper left is the relevant data. Gradient echo images of the left ventricular outflow tract in two orthogonal views demonstrating the aortic insufficiency jet during diastole (arrow). *AAo* ascending aorta, *LV* left ventricle

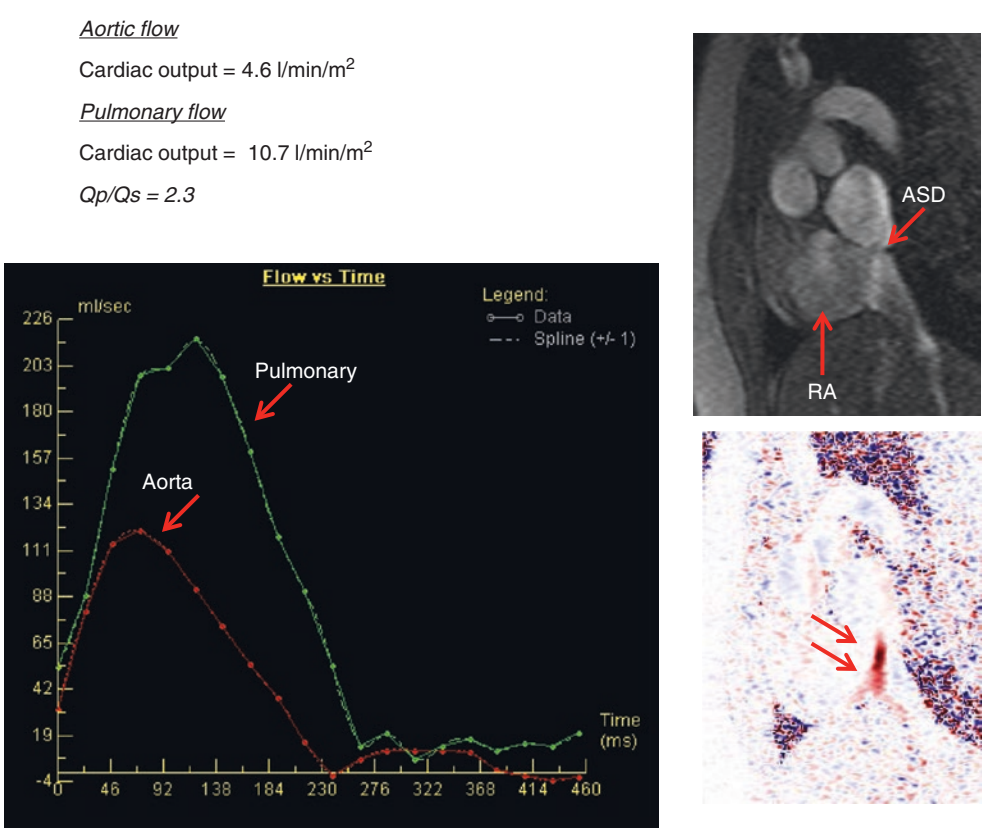

Fig. 1.23 Data and images from a 2-year-old with an atrial septal defect (ASD) of the inferior vena cava type and anomalous right pulmonary venous connections to the right atrium (RA). The off-axis sagittal magnitude image (upper right) demonstrates the ASD while the in-plane, colorized phase-encoded velocity map (lower right) in the same orientation as the magnitude image demonstrates left to right flow by the red color jet as in echocardiography (red is caudad and blue is cephalad flow). The aortic and pulmonary flow are both graphed simultaneously (lower left); data demonstrates as Qp/Qs 2.3

It is key to understand what the "phase" means in the term "phase-encoded velocity mapping" for one to understand how this is used to measure flow. Phase was discussed in the physics section and will be explained in a slightly different way in this section, although it represents the same physical principle. When tissue is excited by radiofrequency energy, the subsequent signal that gets generated when the protons relax (for example, a sine wave) can be described by its frequency (how many cycles per second), its amplitude (the strength of the signal), and its phase (where, in a given time, is the sine wave in its cycle). Two waves can have the same frequency and amplitude but be in different points in their cycle (i.e., they are identical waves but shifted in time); they are out of phase. Think of two identical sine waves placed one atop the other in a signal amplitude-time graph (signal amplitude on the *Y* axis and time on the *X* axis) and then shift one slightly to the right in time; these sine waves are identical but out of phase with each other. Another way to understand this is that the same part of each of the two identical sine wave occurs at a different point of time (e.g., the peak of sine wave "A" occurs prior to the peak of sine wave "B").

The principle underlying phase contrast CMR very simply is that moving tissue within a magnetic field that has a gradient applied to it changes phase. Put another way, whenever anything moves along the axis of an applied gradient, the phase of the spinning vectors in that object becomes altered relative to the stationary object. Remember the Larmor equation states the precessional frequency of the protons is directly proportional to the magnetic field; if that magnetic field is altered by position creating a gradient, the precessional frequency will change depending upon position. Any tissue moving across the gradient will change precessional frequency and accumulate phase shift selectively "labeling" itself. Phase contrast velocity mapping utilizes a "bipolar" radiofrequency pulse which is equal in magnitude but opposite in direction (e.g., turns from positive to negative and then from negative to positive); this is done with two back-to-back pulses with a slight delay. The sequence has the following effect: Before any radiofrequency pulse is applied, protons are tilted as a function of where they are positioned in the magnetic gradient. When the first radiofrequency pulse is applied, both stationary and moving tissue protons are further tilted; when the second equal and opposite radiofrequency pulse is applied immediately afterwards, protons of the stationary tissue return the tilt of their protons back to their original position and accumulate a net phase of zero (their tilt goes back to their original position since they experienced an equal and opposite radiofrequency pulse and haven't moved position—they are experiencing the same magnetic field before and after these pulses). Protons of the moving tissue, however, do not revert to their original tilt since they have moved and are experiencing a different magnetic field because of the magnetic gradient in position. These protons are said to have accumulated a "phase shift." To summarize, this will yield a zero phase change for stationary objects when both pulses are applied whereas there will be a net accumulation of phase in moving tissue. By subtracting, pixel by pixel, the phases of one pulse from the other, background phase changes of stationary objects are canceled out and the phase shift of the moving tissue is amplified. Then, usually, the "phase difference" method is used to map the phase shift angles into signal intensities. Flow is calculated by the formula:

$$\Delta \text{phase} = g \times v \times T \times A_g$$

where g = gyromagnetic ratio, v = velocity, T = duration of the gradient pulse and A_g is the area of each lobe of the gradient pulse.

By tailoring the strength of the radiofrequency pulse to the anticipated velocities, accurate measurement can be obtained; this is called a VENC (velocity encoding) and is the equivalent of the Nyquist limit in echocardiography. Using the VENC and the signal intensity, the velocity of moving tissue in each pixel can then be encoded. This can occur with either blood (hence blood phase-encoded velocity mapping) or with myocardial tissue (also called myocardial velocimetry and is the equivalent to Doppler tissue imaging).

As mentioned, spatially, there are two ways to encode velocity in the image: (a) "through plane" where each pixel encodes velocity into and out of the plane of the image and (b) "in-plane," where velocities are encoded in the plane of the image and not into and out of the plane similar to Doppler echocardiography. Unlike Doppler echocardiography, however, velocities are encoded in either the *Y*- or *X*-direction of the image. This is advantageous as each pixel can encode velocity in three orthogonal planes. Motion in one direction is mapped onto the anatomic image as increased signal intensity or bright and motion in the other direction appears signal poor and dark; stationary tissue appears gray. Air, such as in the lungs or around the patient, is encoded in a mosaic black and white. Color can be added to make it similar to Doppler echocardiography.

Flow measurements by this methodology utilize the cross-sectional area of the vessel perpendicular to the transaxial direction of flow. All software can identify the regions of interest simultaneously on the anatomic or "magnitude" images as well as the "phase" images (which can sometimes be difficult to read). The product of the velocity and the area of an individual pixel give flow through that pixel; summing this across the vessel cross-sectional region will yield the flow at a given phase of the cardiac cycle. Integrating this across the entire cardiac cycle (i.e., each phase plotted as a time-flow curve), the flow during one heartbeat is calculated. The product of the heart rate and this flow in one heartbeat will yield the cardiac output.

Through plane phase-encoded velocity mapping can also be used to assess the peak velocity for gradient calculations as might be used for coarctation of the aorta or ventricular pressure estimates as with a tricuspid regurgitant jet. If the plane is perpendicular to flow in the region of maximum velocity, the greatest velocity in any pixel in the region of interest in the cardiac cycle is used in the simplified Bernoulli equation. It should be noted that planes not perpendicular to flow or one at a level where the maximum velocity is not present will underestimate this number; generally, this is used in conjunction with in-plane velocity mapping (see below) to measure maximum velocities. This is similar to Doppler echocardiography where, if the plane is angled obliquely to the jet of interest or the sector is not in the area of maximum velocity, an underestimate of the maximum velocity will occur.

Encoding velocity parallel to flow ("in-plane" velocity encoding) is predominantly used to measure peak velocities which is similar to what Doppler echocardiography measures. The advantage of this type of phase encoding over the through plane technique in measuring maximum velocities is that velocities can be measured along a jet of interest in the direction the jet is pointing (similar to continuous wave Doppler), through plane mapping is placed at a certain level of the jet and the velocity measured which is similar to the range-gating technique of pulse wave Doppler echocardiography. With in-plane velocity mapping, the jet is aligned by rotating the entire field of view to make one side exactly perpendicular to the jet. The peak flow velocities can then be translated into pressure gradients via the simplified Bernoulli equation. The phase maps on present-day scanners can give a temporal resolution of about 15–20 ms with non-breath-hold techniques.

Phase-encoded velocity mapping has limitations. Reliability of both through plane and in-plane velocity mapping is a function of a few factors such as slice thickness ("partial volume" effects may induce inaccuracies in velocity calculations) and the angle of the jet (the jet needs to be aligned perpendicular to the direction of phase encoding, similar in some sense, to Doppler flow measurements). In addition, if the VENC is not chosen close but not below the maximum velocity anticipated, errors may occur. If the VENC chosen is too low, velocities in the vessel will exceed the ability of the CMR scanner to encode them which is akin to aliasing and exceeding the Nyquist limit in Doppler echocardiography. If the VENC chosen is too high, the lower velocities will not be measured as accurately as well as signal to noise decreasing; this is analogous to the difference when measuring a 4 oz of fluid in a 6 oz measuring cup (appropriate setting of the VENC) versus a gallon measuring cup (in appropriate setting of the VENC). Maxwell terms, eddy currents, and whether or not background subtraction is used will also play a role in velocity mapping accuracy.

Finally, by combining through plane and in-plane velocity mapping into the same sequence, CMR can acquire a 3-dimensional slab of velocities termed 4-dimensional or "4D flow" meaning three dimensions of space plus time [47, 48]. Using modern-day gradients and advanced software such as compressed sensing, the entire heart and great vessels can be acquired in anywhere from 3 to 8 min. There are multiple vendors with excellent software that can qualitatively visualize and quantitatively assess these datasets (Fig. 1.14).

There are multiple advantages to 4-D flow including being able to "go back" to any blood vessel in the thorax after the patient exam has ended to measure flow; 2D PCMR is aimed at one vessel at a time and once the patient leaves the scanner, there is no one to measure flow in another vessels. In addition, all vessels are measured at the same average heart rate as opposed to 2D flow where it is generally different, making 4D flow more consistent. Further, flow profiles in blood vessels and the heart and their interactions in 4D are easily visualized by this methodology. There are even implementation of these sequences where cine imaging and flow can be acquired at the same time, obviating the need for cine imaging and anatomic imaging (generally with the addition of a contrast agent however) [49]. Finally, metrics such as pulse wave velocity, pressure drop, and energy loss can be calculated whereas with 2-D PCMR, it may be difficult to impossible to do so (see below).

There are drawbacks to 4D flow as well. For some implementation of these sequences, administering a contrast agent such as gadolinium or ferumoxytol (see MRA section below) is useful for better signal to noise.

PCMR by 2D has many applications in congenital heart disease and in broad categories, they are (a) flow quantification, (b) flow visualization, (c) velocity measurements, and (d) myocardial velocimetry.

1.8.5.1 Flow Quantification

1. Cardiac Output (Figs. 1.22 and 1.23): Measuring cardiac output is an essential factor in assessing cardiovascular performance; this is especially true in patients who have undergone surgical procedures or who have undergone catheter intervention. Lesions such as single ventricles, corrected transposition, tetralogy of Fallot, etc. all benefit from measuring an elementary parameter such as cardiac output. This can also be used as an internal check to the ventricular stroke volume measurements.
2. Regurgitant Lesions (Fig. 1.22): As flow can be quantified as forward and reverse flow, the regurgitant volumes and fractions can be measured and calculated; lesions such as tetralogy of Fallot after repair with a transannular patch [50] or in patients with a bicuspid aortic valve and severe aortic insufficiency all require measurement of

leaky semilunar valves. These measurements are readily obtained by placing phase-encoded velocity map at the sinotubular junction (for the aortic valve) and just above the pulmonary valve and measuring the forward and reverse area under the flow-time curve. The regurgitant fraction is simply the area under the reverse flow (regurgitant volume) divided by the area under the forward flow (forward volume) multiplied by 100. An internal check is the measure flow in the cavae which should be the net cardiac output measured by velocity mapping in across the leaky semilunar valve. To obtain how much leakage there is across an atrioventricular valve, a combination of techniques are used; cine CMR is used to measure the stroke volume of the ventricle and phase-encoded velocity mapping to measure the amount of forward flow through the semilunar valve. The difference between the two (with no intracardiac shunts) is the regurgitant volume of the atrioventricular valve. Alternatively, the forward flow across the atrioventricular valve during diastole and the net flow across the semilunar valve in systole can be used (assuming no shunting).

3. Shunts (Fig. 1.23): Many lesions in congenital heart disease have shunting between the circulations present; this shunt flow can be easily calculated by placing velocity maps across the aortic valve and main pulmonary artery and measuring flow (e.g., Qp/Qs) [51]; if there is a aortopulmonary window, branch pulmonary artery flow is generally used instead. Measuring flow in both branch pulmonary arteries can add an internal check on the amount of pulmonary blood flow for intracardiac shunts and the sum of the flow in the cavae can be used as a check on the amount of systemic blood flow.
4. Flow Distribution to Each Lung: [52] Altered flow distribution to left and right lungs can be common in many lesions in congenital heart disease such as in single ventricle lesions after Fontan, tetralogy of Fallot, or in transposition of the great arteries after arterial switch procedure; all may have branch pulmonary stenosis. Relative flow to each lung is assessed by placing a phase-encoded velocity map at each branch pulmonary artery although care must be taken to place the map in the branch pulmonary artery proximal to the takeoff of the first branches to ensure this blood flow is included. Flow measured in the main pulmonary artery must equal the sum of the flows to each lung in the absence of collaterals and is used as an internal check.
5. Collateral Flow: [53] Patients with single ventricles after bidirectional Glenn or Fontan operation develop aortopulmonary collaterals presumably in response to decreased pulmonary blood flow and cyanosis [54]. In addition, patients with relatively long-standing coarctation of the aorta can develop aortic collaterals which bypass the obstructed segment. In the former, the amount of collateral flow can be quantified in two ways: (1) by measuring flow via velocity mapping across the ventricular outflow tract and subtracting measured caval return and (2) measuring flow in the pulmonary veins and subtracting measured flow in the branch pulmonary arteries. In coarctation, the amount of collateral flow can be determined by placing a phase-encoded velocity map across the aorta just distal to the coarctation site and across the aorta at the level of the diaphragm. Normally, flow at each level will be very similar or the flow at the level of the diaphragm slightly lower (because of flow to the intercostal arteries); however, in the presence of coarctation with collaterals, flow just distal to the coarctation site in the aorta will be lower than flow in the aorta at the level of the diaphragm since collateral flow will present in the latter and not in the former.

1.8.5.2 Velocity Measurements

1. Pressure Gradients: Stenoses of a blood vessel such as a great artery (e.g., coarctation of the aorta, left pulmonary artery stenosis, or a pulmonary artery band, Fig. 1.21) or of a valve (aortic stenosis in a bicuspid aortic valve) can occur in numerous congenital heart lesions. It is important for many reasons to determine pressure gradients in these lesions; as noted above, the determination of gradients by CMR is similar to Doppler echocardiography, using the simplified Bernoulli equation. A maximum velocity is measured, typically in the vena contracta, and the gradient is simply the product of 4 and the velocity (in meter/second) squared. Measurement of maximum velocities may be performed in two ways: (a) "in-plane" velocity mapping directed parallel to the obstruction to flow and (b) "through plane" velocity mapping perpendicular to flow. Both have their strengths and weaknesses (see above discussion).

1.8.5.3 Flow Visualization

1. Septal Defects Using In-Plane Velocity Mapping: Septal defects at both the atrial and ventricular level can be visualized with i2D *n*-plane velocity mapping. The imaging plane needs to be oriented in the direction of the flow across the defect to successfully visualize it; blood flowing one way would be dark and flow the other way would be bright. In addition, color can be superimposed on the image to simulate color Doppler echocardiography.
2. Flow Directionality in Blood Vessels Using Through Plane Velocity Mapping: A good example of this is isolation or disruption of the subclavian arteries; this may be caused by surgery (e.g., a subclavian flap angioplasty to

repair coarctation of the aorta) or may be congenital. When this occurs, the subclavian artery usually is supplied with blood in a retrograde fashion via the vertebral artery; sometimes, with some paraspinal plexuses or other collaterals supply the subclavian artery. Clinically, a "subclavian steal" can occur and CMR velocity mapping techniques can be used to identify retrograde flow in the vertebral arteries. Normally, if an axial through plane velocity map is placed in the neck, both carotid and vertebral arteries will be labeled as either bright or black on the images as they are all flowing in the same direction. With isolation of a subclavian artery, flow in the ipsilateral vertebral artery is retrograde while flow in the other three head vessels (carotid and vertebral arteries) will be antegrade. A velocity map in this scenario will encode the vertebral artery ipsilateral to the isolated subclavian artery in one direction (e.g., dark) and the other three head vessels will be encoded in the opposite direction (e.g., bright), proving the physiology.

3. Valve Morphology (Fig. 1.13): Phase contrast velocity mapping is also useful for identifying valve morphology; as through plane phase contrast velocity mapping "tags" flowing blood, this can be used to outline the leaflets tips making a cast of the valve morphology while it opens and closes; the flowing blood is bright or dark and highlights the valve leaflet tips which are gray. Bicuspid, unicuspid, and quadricuspid valves are easily seen. Of particular note, bicuspid aortic valve is very common clinically; it can easily be identified by phase contrast mapping and the degree of valvular stenosis and regurgitation assessed [55, 56].

1.8.5.4 Myocardial Velocimetry

This application of phase contrast velocity mapping is the CMR equivalent to Doppler tissue imaging in echocardiography; velocities of the myocardial tissue can be recorded. The phase contrast velocity mapping sequence is configured such that the VENC is set fairly low (15–30 cm/s); modifications in the sequence must be made to keep the TE as low as possible. Doppler tissue imaging can only record myocardial velocities in one direction; that is parallel to the Doppler beam. Myocardial velocimetry, however, is a much more comprehensive measurement of myocardial velocities in that, similar to other phase contrast velocity mapping applications, each pixel can encode velocities in three orthogonal planes; a 3-dimensional velocity map of the myocardium can be measured. Both myocardial velocimetry in CMR and Doppler tissue imaging in echocardiography suffer from the same drawback in that both techniques do not truly measure the velocity of a specific piece of myocardium; they identify a point in space and the velocity of myocardium moving into and out of that point is measured. Only CMR myocardial tagging and Doppler spectral tracking truly measure the velocity of a piece of myocardium noninvasively. An excellent review comparing the merits of myocardial velocimetry to myocardial tagging was published in 1996.

4D flow imaging has found utility in multiple applications in congenital heart disease [57]. All the above-mentioned metrics with 2D flow can also be calculated and visualized by 4D flow, especially visualizing shunts or regurgitant fraction. In addition, however, pulse wave velocity, which has a bearing on aortic stiffness and ventricular performance, can be obtained easily by multiple 4D flow methodologies [58]. Pressure flow fields and pressure drops across the entire aorta can also be calculated and can come in very useful in lesions such as coarctation of the aorta [59]. In addition, wall shear stress can be derived from 4D flow images in the aorta in patients, for example, with a bicuspid aortic valve [60]. Finally, as a last example, new metrics such as energy loss can be measured and assessed in congenital heart disease, such as in the single ventricle [61] (Fig. 1.14).

1.8.5.5 Magnetic Resonance Angiography (MRA) (Figs. 1.20, 1.21, 1.24, and 1.25)

Magnetic resonance angiography, most based on intravenous gadolinium diethylenetriamine pentaacetic acid (Gd-DTPA), can determine detailed anatomy such as major pulmonary and systemic arteries and veins and to glean physiology is a key part of the examination. As discussed above, gadolinium is a paramagnetic element which is administered in a chelated form and is an extracellular agent that changes the magnetic property of the tissue or vessel it is in. It markedly decreases T_1 relaxation and which allows its application to distinguish the target structure (e.g., the aorta) from background (e.g., lung, other mediastinal contents). It is considered a highly safe substance with adverse events occurring in one in 200,000–400,000. Usually a "double dose" of contrast is given (for most agents, this is 0.4 cm^3/kg; please check the labeling of your individual agent).

In the past, much attention has been given to the incidence of nephrogenic systemic fibrosis (NSF) in patients with chronic, severe renal failure, first described in 2000 in 15 patients undergoing hemodialysis who presented with "scleromyxoedema-like" skin lesions. A detailed discussion of this entity is beyond the scope of this chapter; suffice it to say that after modifications of gadolinium use, NSF is nearly eradicated. Very few reports of children developing NSF exist and none under 6 years of age.

In addition, there have also been reports of linear gadolinium contrast agents accumulating in small amounts in the brain of individuals exposed to more than four doses of the agent. The recent FDA communication on this issue states that although more testing is needed, data supports the notion that no adverse effects are noted from this issue.

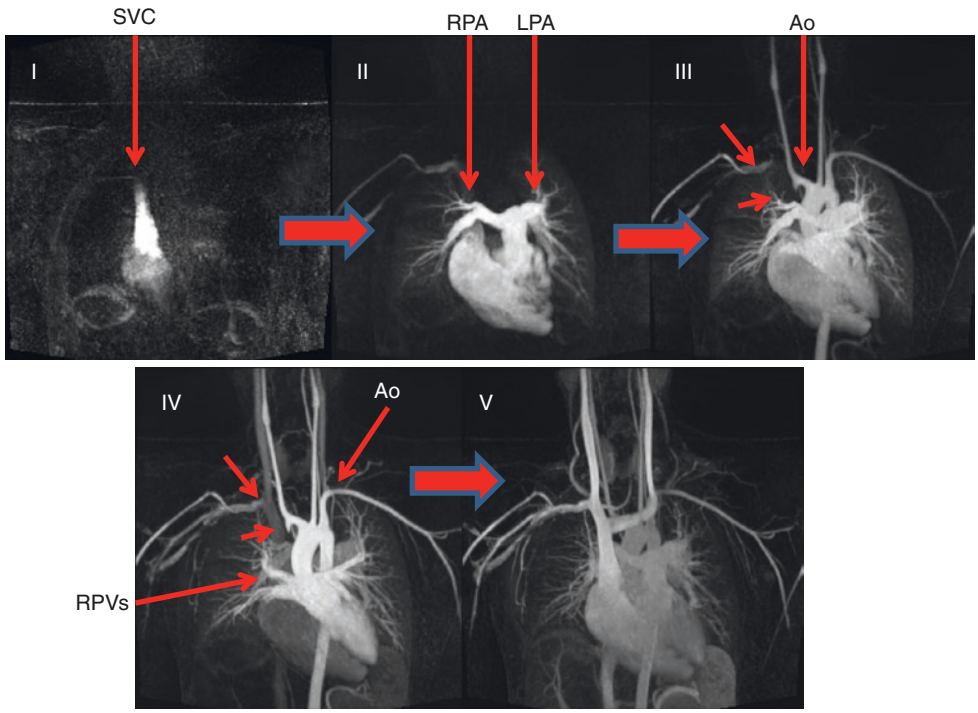

Fig. 1.24 Three-dimensional time-resolved gadolinium imaging in a coronal view. The images are maximum intensity projections (MIPs) and temporally follow the roman numeral from left to right and from top to bottom. Each phase can be created into a 3-dimensional image. Spatial resolution is an isotropic 1 × 1 × 1 mm and temporal resolution is 2.2 s. In I, flow into the superior vena cava (SVC) is seen followed by flow into the right side of the heart (II). In III, flow is now seen in the pulmonary veins and the beginnings of the aorta (Ao). In IV, flow has left the right side of the heart and is now mostly in the pulmonary veins, the left side of the heart, and the aorta. In V, flow is seen returning to the heart from the systemic veins. Note the interrupted right subclavian artery in III and IV (arrows). *LPA* left pulmonary artery, *RPA* right pulmonary artery, *RPVs* right pulmonary veins

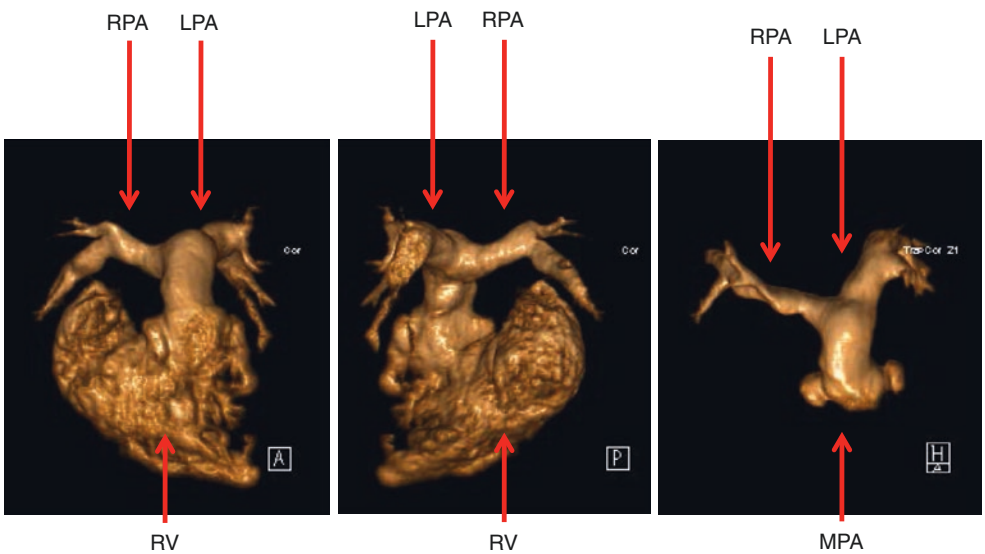

Fig. 1.25 Three-dimensional right heart reconstructions of the patient in Fig. 1.24. The right ventricle (RV), main (MPA), right (RPA), and left pulmonary artery (LPA) are clearly seen from an anterior (left), posterior (middle), and transverse (right) view. The RV was removed from the transverse view (right) to facilitate visualizing the branch pulmonary arteries

This can be performed anytime during the examination; however, it is performed after cine imaging. It can be performed before or after PCMR; however, if performed before PCMR, the contrast agent boosts the signal of the PCMR flow sequence, giving better signal to noise and more robust data. Since approximately 10 min is needed between gadolinium administration and imaging for delayed enhancement and even more for T_1 mapping (see below), the time after gadolinium administration but before viability imaging is used to perform either phase contrast velocity mapping or

3-dimensional static inversion recovery gradient echo imaging (see below). There are two types of contrast-enhanced techniques commonly used to evaluate 3-dimensional anatomy:

1. Static 3-dimensional imaging can be utilized to create a 3-dimension image of the cardiovascular system which can be rotated and cut in any plane desired. The 3-dimensional slab (see Physics section) can be acquired in any orientation and can be viewed in its raw data format, as a maximum intensity projection, a shaded surface display, or as a volume rendered object. As it is a 3-dimensional acquisition with one frequency encoding and two phase encoding directions, the thickness of the slices can be much thinner than other techniques—on the order of ¾ to 1 mm. As the resolution is higher than other techniques in CMR, this type of imaging is used to visualize smaller vessels (e.g., aortic-pulmonary collaterals in pulmonary atresia/intact ventricular septum, aortic collaterals in coarctation, etc.). Multiple 3-dimensional data sets are generally obtained which (a) can separate out the systemic and pulmonary circulations and (b) increases the chances of successfully imaging what is needed.

   Older techniques relied on knowing exactly when the contrast agent reaches the target vessel to begin the 3-dimensional sequence. This was performed in either two ways: (a) Bolus tracking, where the target structure (e.g., the pulmonary arteries in the case of tetralogy of Fallot) is imaged with "real-time" sequence during gadolinium injection—once the contrast agent is seen to arrive at the target structure, the 3-dimensional sequence is then obtained. (b) Timing bolus, where a small amount of contrast agent is injected and timed to determine when it will arrive at the target vessel. Injecting the full dose of gadolinium followed by the 3-dimensional sequence with a delay placed based on the small amount of contrast agent initially given is then performed knowing the gadolinium will arrive at the target vessel based on the initial timing bolus. Modifications need to be made, depending upon the 3-dimensional sequence, if it is "center weighted *k*-space" or "front-loaded *k*-space."

   The current state of the art is performing a static 3D sequence (inversion recovery gradient echo imaging with ECG gating utlizing the navigator technique and respiratory motion adaptation) either immediately after time-resolved imaging (see below) or with the "slow-drip" of gadolinium technique (which finishes administering gadolinium in the first 1/3 of the sequence) [62]. The navigator technique uses a coil to monitor the diaphragm and allows the algorithm to accept all the data within a certain range of where the diaphragm is (2–4 mm), adjust as needed, and discard the rest. In this way respiratory motion is compensated for. This 3D technique is generally done isotropic and can be performed with resolutions as low at 0.6 mm using ferumoxytol (see below). Newer techniques under study now allow for creating 3D images without the need for a navigator and the sequence monitors the motion of the heart itself, not rejecting any imaging data at all [63].
2. Time-resolved (dynamic) 3-dimensional gadolinium imaging (Fig. 1.24) is similar to the static version mentioned above; however, multiple 3-dimensional data sets are obtained in an extremely short period of time (subsecond). These 3-dimensional data sets are acquired continuously and the bolus of gadolinium is followed through the cardiovascular system. This can be performed successfully with parallel imaging (multiple coils used), strong gradients and slew rates, and advanced software and sequences. Each phase of the acquisition can be made into a high-resolution (1 mm or less isotropic voxels) 3-dimensional image. This approach can be used to image physiology (view shunt flow or small connections) as well as determining lung perfusion (e.g., regions of lung with higher flows will be much brighter than regions of lung with low flow or no flow such as with pulmonary embolism).

   In either technique, it is recommended, as best as possible, to acquire isotropic voxels (voxels with the same dimensions in all three directions). When acquiring the data in this manner, the 3-dimensional image can be manipulated and resliced in any plane and the resulting image would appear as if it was acquired in that orientation. In neonates and infants where smaller spatial resolution is needed, isotropic voxels are also very important but signal to noise takes on a very important role; as long as the voxel sizes are small, the field of view can remain high (i.e., by keeping the matrix high) and signal to noise will be preserved.

   The advent of a new iron-based contrast agent, ferumoxytol, had changed the game in pediatrics. It has a long half-life of approximately 14 h which means that high-resolution imaging can be done in a longer period of time without loss of signal (as opposed to a first pass technique like cardiac catheterization angiography or ultrasound contrast agents). In a large-scale multicenter safety trial, it has been found safe in children as well as adults [21]. Using the free breathing 3D inversion recovery gradient echo sequence, resolutions of 0.8 mm can be easily reached in less than 5–7 min in young patients, visualizing coronaries in neonates and creating 4D cine images [20]. With the ability to maintain signal, both respiratory and cardiac phases can be imaged, yielding 4D cine imaging at different phases of the respiratory cycle without the need for a navigator for the diaphragm [18].

1.8.5.6 Viability (Delayed Enhancement) (Figs. 1.7 and 1.10) [64]

It is generally believed that infarcted myocardium is less of an issue in congenital heart disease than it is in adults and there is some truth to this—but just some. Many lesions in pediatric cardiology, either in the native state or postoperatively, are at risk for myocardial necrosis. The list of diseases that may manifest discrete myocardial scarring can be divided into three large categories and examples given below.

1. **Native coronary lesions** such as anomalous left coronary artery from the pulmonary artery or from the opposite sinus or coronary fistula or sinusoids in lesions such as pulmonary atresia with intact ventricular septum.
2. **Surgical coronary manipulation/postsurgical lesions** such as transposition of the great arteries after arterial switch operation or after a Ross operation where coronaries are manipulated or patients with single ventricle or repaired tetralogy of Fallot.
3. **Acquired pediatric heart disease** such as Kawasaki's disease, myocarditis, or dilated cardiomyopathy.
4. **Native myocardial lesions** such as hypertrophic cardiomyopathy, Duchenne's muscular dystrophy, and in tumor characterization (e.g., fibroma).

CMR viability imaging, also known as delayed enhancement, has shown to be effective in the detection of myocardial scarring and can be applied to the infant through adult with congenital heart disease [65–67]. With viability imaging, intravenous gadolinium chelate, which can freely distribute in extracellular water but cannot cross intact cellular membranes, is delivered to the myocardium and accumulates in areas of fibrosis due to increased volume of distribution and slower washout kinetics [68]. This imaging technique distinguishes areas of myocardial scarring with high signal intensity in comparison to viable myocardium.

As examples, many studies have used delayed enhancement to correlate myocardial scarring with heart function and clinical outcome in different diseases. Babu-Narayan et al. correlated delayed enhancement in transposition of the great arteries patients after surgical repair with age, length of time after surgery, higher right ventricle end-systolic volume index, and lower RV ejection fraction [69]. Babu-Narayan et al. also showed correlation of scarring with increased QRS duration, QT dispersion, and JT dispersion from ECG exams as well as a significantly higher occurrence of arrhythmia/syncope. Myocardial scarring has also been investigated in tetralogy of Fallot patients after repair [70, 71]. RV delayed enhancement was shown to correlate with decreased exercise tolerance, increased RV indexed end-systolic volume, decreased RV ejection fraction, and more documented clinical arrhythmia. Left ventricular delayed enhancement correlated with more arrhythmia, shorter exercise duration, increased LV indexed end-diastolic and end-systolic volume, and decreased LV ejection fraction. Regions of myocardial delayed enhancement have also been known to occur in patients with hypertrophic cardiomyopathy [72, 73] and the extent of delayed enhancement has been associated with clinical markers of sudden death risk and progression to heart failure [74].

Regions of irreversible myocardial injury will exhibit high signal intensity on T_1-weighted images when administered gadolinium which significantly shortens the longitudinal relaxation time. Although the mechanism by which this occurs is open to debate, it is thought that ruptured cell membranes of myocytes allow the gadolinium to be avidly taken up by the scarred myocardium into the intracellular regions; this results in increased tissue concentration of the contrast agent and, hence, an increased signal intensity. In addition, with scar tissue, there is increased interstitial space between collagen fibers, allowing for gadolinium to inculcate itself in these regions and become more concentrated. This is opposed to normally perfused myocardium where the gadolinium is subsequently "washed" out by coronary blood flow. The signal intensity-time curves separate, with the infarcted myocardium gadolinium curve becoming signal intense much before perfused myocardium and remaining highly signal intense after 5–20 min whereas normal myocardium becomes much less so. CMR pulse sequences, first described in the literature in the mid-1980s, have taken advantage of this high concentration and slow washout of contrast agent when attempting to image infarcted myocardium. With segmented inversion recovery fast gradient echo sequences and other techniques such as steady-state free precession, signal intensity differences between normal and infarcted myocardium can be as high as 500%. The technique has been shown to accurately delineate the presence, extent, and location of acute and chronic myocardial infarction.

After preliminary scout images and cine sequences are obtained, 0.1–0.2 mmol/kg of intravenous gadolinium is administered. The myocardium is then imaged approximately 5–20 min after this injection; as neonates and children wash out the contrast agent quicker, they are usually imaged on the "sooner side" or if imaged later, have a longer inversion time (TI) (see below). The sequence makes use of a nonselective 180° inversion pulse which spoils all the spins in the myocardium (black on the image) and gives it T_1 weighting. The magnetization of tissue goes from +1 to −1 by this process. As both the myocardial and scar tissue begin to recover their spins (enabling the myocardial and scar tissue to "give off" signal), because scar tissue shortens the T_1, it recovers signal much quicker than normal myocardium. A time delay is placed after the 180° inversion pulse (TI) to image the ventricle at just the point where the normal myocardium is about to regain signal again (and because the scar tissue recovers spins much quicker, can give off signal). That

is to say that the TI is chosen between the nonselective 180° pulse and the center of *k*-space of the sequence so that the magnetization of normal myocardium is near the zero line (i.e., normal myocardium is dark on the image). This allows for maximizing the difference in signal intensity between scared and normal myocardium; the ventricle is imaged in mid-late diastole. TI time can be manually changed as the acquisition time continues. Collections of lines of *k*-space generally occur every other heartbeat.

There are a number of recent advances that have further refined the ability of CMR delayed enhancement to detect myocardial fibrosis. Some manufacturers have implemented 3-dimensional volumes slabs to allow for thinner slices. Steady-state free precession imaging can be used as opposed to gradient echo imaging to decrease the time needed for image acquisition. In addition, "single-shot" techniques are available (as opposed to segmented versions) to obtain an entire slice in one heartbeat, further allowing for increased coverage of the myocardium in one breath-hold. Motion-corrected viability imaging with high signal intensity as well as wideband viability imaging allows for improved fidelity of the images as well as compensating for motion and metallic artifact respectively.

Further advances have relied on refining the correct TI time which, as can be surmised, is a critical component to the whole procedure; as mentioned, it is chosen to optimally "null" the myocardium (i.e., the time at which normal myocardium crosses the "zero" point of signal intensity) where the difference in signal intensity between normal and infarcted tissue is maximized. With a TI time that is too short, the normal myocardium will be below the zero point which will cause two issues (a) differences between signal intensities of infracted and normal myocardium will not be maximized and (b) as the image intensity is a function of the magnitude of the magnetization vector, normal myocardium may become hyperenhanced and scar tissue may become nulled if the TI is shortened enough. On the other hand, if the TI time is too long, the normal myocardium will be shades of gray with the scar tissue having high signal as well; as one can see, the contrast between the two tissues will be reduced. Finally, as mentioned already, as gadolinium concentration decreases from the myocardium as time progresses, the TI will have to be adjusted upwards the longer the time after injection.

To make better choices of TI times, two advances have improved the process: (1) "TI scouts" have been developed which obtain images at various increments of TI. The imager can choose the TI based on this scout as to image which appears optimal. (2) A phase-sensitive inversion recovery approach can be used which provides consistent contrast between normal and scarred tissue over a wide range of TIs. This "auto viability" technique maintains signal polarity; the inversion recovery preparation pulse and phase reference acquisition are interleaved requiring 2 heartbeats.

There are a few pitfalls with viability imaging. In patients who cannot hold their breath or with arrhythmias, using certain viability sequences, image quality can be degraded although with single-shot viability imaging and motion-corrected versions, this is less of an issue. In addition, ghosting artifacts can occur from tissue which have long T_1 values, such as pericardial effusion.

1.8.5.7 Multiparametric Mapping (Fig. 1.8)

One of the strengths of CMR is the ability to characterize tissue such as discrete fibrosis or tumor characterization. T_1, T_2, and T_2 star mapping has emerged as extensions of this capability which allows for spatially assessing the relaxation times of each one of these spin properties to assess for diffuse fibrosis (extracellular volume), myocardial edema, or iron deposition respectively. A disproportionate accumulation of collagen in the heart is an important factor in the etiologies of heart failure, diastolic dysfunction, and sudden cardiac death or as a result of valve lesions such as aortic stenosis and this generalized increase in collagen can be measured by the T_1 relaxation time. Similarly, assessment of myocardial edema in regions near infarcts or in inflammatory states such as myocarditis would be useful to identify and this can be measured by T_2 mapping. By the analysis of T_2* in patients who may have iron overload (thalassemia, sickle cell disease, etc.), the amount of myocardial iron present can be measured.

There are multiple papers which describe these techniques in great detail which is beyond the scope of this chapter and the reader is referred to them [75–77]. The general concept behind, for example, T_1 mapping, is acquiring many images with different T_1 weightings, and the signal intensities in each are fit to the equation for T_1 relaxation. To be more specific, the magnetization of the tissues/spins are either inverted or nulled with a radiofrequency pulse, and the T_1-weighted images acquired at different T_1 times or times after the inversion or saturation. By doing this over multiple heartbeats and allowing for the tissue to relax, in between a series of tissue excitations, a T_1 relaxation curve can be created. When this is performed prior to gadolinium administration (native T_1 relaxation time) and after gadolinium (post contrast T_1 relaxation), with a blood hematocrit, the extracellular volume may be calculated as a percent by:

$$\mathrm{ECV} = \left(1 - \mathrm{hematocrit}\right) \frac{\dfrac{1}{\mathrm{postcontrast}\, T_1\, \mathrm{myo}} - \dfrac{1}{\mathrm{native}\, T_1\, \mathrm{myo}}}{\dfrac{1}{\mathrm{postcontrast}\, T_1\, \mathrm{blood}} - \dfrac{1}{\mathrm{native}\, T_1\, \mathrm{blood}}}$$

An estimate of the hematocrit from the images, also termed "synthetic hematocrit," has been touted to be a good substitute for a blood drawn hematocrit [78] but this is con-

troversial [79]. Similar techniques are used for T_2 and T_2 star but without the use of gadolinium. In the CMR protocol, T_1 mapping is performed prior to gadolinium administration and then approximately 15 min afterwards or generally a few minutes after viability imaging.

T_1 mapping has found utility in multiple areas of pediatric congenital and acquired heart disease. For example, in tetralogy of Fallot, expansion of the extracellular space in both the right and left ventricles is present [80, 81] and expansion of left ventricular extracellular space in adult tetralogy of Fallot patients has been linked to adverse events [82].

Similarly, T_2 mapping for edema has found utility in the adult world in acute ischemia and in both the pediatric and adult world as one of the criteria for myocarditis [83]. Generally, values over 55–60 ms at 1.5 T are considered abnormal.

T_2* for Myocardial Iron Assessment In brief, the sequence obtains multiple images of the same short axis slice at various echo times utilizing a gradient echo sequence. With longer TEs, the myocardium and liver become increasingly dark. Because iron is ferromagnetic, the magnetic properties of the myocardium and liver change with increasing iron concentration, decreasing the measured T_2* (which makes the myocardium even darker) relative to normal myocardium. Values <20 ms are considered at risk for decreased ventricular function. Chelation therapy is generally modified in these patients using this information.

The combination of these techniques of multiparametric mapping can be utilized in a whole host of other diseases. Literature on amyloidosis, Fabray's disease, and non-ischemic cardiomyopathy has all been published.

1.9 Other Sections of the CMR Protocol

There are a number of other techniques in CMR that are not infrequently used but do not fit into the generalized protocol. They should be inserted at appropriate points in the protocol.

1.9.1 Coronary Artery Imaging (Fig. 1.6) [84, 85]

For CMR to be implemented successfully to image the coronary arteries, two main technical challenges need to be overcome; that of cardiac motion and respiratory motion. The magnitude of both motions greatly exceeds coronary artery diameters and in the absence of motion suppression algorithms, would cause blurring and possibly missing the coronary arteries all together. There are multiple other challenges as well but these two present the most complex ones. Various techniques have been used in the past to overcome these motion-related problems and a history of how modern coronary imaging is performed by CMR is beyond the scope of this chapter; suffice it to note that it has been a long road to the present-day high-quality, high-resolution imaging of the coronary arteries.

To compensate for coronary motion, high-quality ECG or vector gating is required; peripheral pulse gating would not be adequate. In addition, if arrhythmias were present and "arrhythmia rejection" algorithms not used, image degradation will be present. In either case, cardiac motion is compensated for by imaging during the "quiescent phase" of the cardiac cycle which is generally mid to late diastole or if the patient has a high heart rate (generally >100 beats/min), end-systole. End-systole is advantageous as well in that this is the phase where the coronaries are most filled with blood. To determine the "quiescent phase" of the cardiac cycle, it has been our practice to perform a 4-chamber view and left ventricular outflow tract high temporal resolution cine (30–60 phases depending upon the heart rate), focusing on the atrioventricular groove and aortic annular motion respectively. When both of these regions are motionless should be considered the beginning of the "quiescent phase." In addition, the length of the "quiescent phase" is measured in both views as well and is timed only as both structures remain motionless; this is helpful in determining how long the "shot time" for each heartbeat is (i.e., the amount of time it takes to acquire the lines of *k*-space).

To compensate for respiratory motion, a number of approaches have been used in the past including breath-holding, chest wall bellows, etc.; however, in the current era, the state of the art is utilizing navigator pulses. A navigator is used to track motion of a structure and, in this particular instance, is used to determine respiratory motion. Most navigators in use today for coronary imaging track the right dome of the diaphragm; however, the left hemidiaphragm and the anterior chest wall have also been used. Lines of *k*-space accepted into image reconstruction are only those that occur when the diaphragm is within certain defined boundaries (i.e., within 2 mm of the end-expiratory position of the diaphragm). Efficiency is the amount of lines of *k*-space accepted divided by the total lines of *k*-space. The overwhelming effect of respiration on cardiac motion is in the supero-inferior dimension and at end-expiration, the ratio between cardiac and diaphragmatic displacement ranges from 0.6 to 0.7 and this "tracking factor" is used to shift slice position coordinates. Newer sequences in development currently track the actual motion of the heart and as such, data from every heartbeat is acquired yielding an efficiency of 100% [18].

Finally, two other major pre-pulses are used to suppress the signal from surrounding tissue. As fat has a relatively short T_1, a frequency selective fat prepulse can be used to saturate the signal from fat surrounding the coronaries.

Because the coronaries also course near the epimyocardium, cardiac muscle needs to be suppressed as well. Unfortunately, blood and myocardium have similar T_1 relaxation properties; however, their T_2 relaxation differs significantly. T_2 preparation pulses are used to enhance the contrast between the blood of the coronaries and the myocardium (it also suppresses deoxygenated venous blood); magnetization transfer contrast is used to image coronary veins.

Uses in congenital heart disease fall into three basic categories: (a) anomalous coronary artery imaging such as anomalous left coronary artery from the pulmonary artery or anomalous coronary arteries from the opposite sinus, (b) patient who have had coronary manipulation surgically such as transposition of the great arteries after arterial switch or the Ross procedure, and (c) acquired coronary artery disease such as Kawasaki's disease or with familial hypercholesterolemia.

1.9.2 Perfusion Imaging (Fig. 1.9)

Perfusion imaging of the myocardium with CMR using contrast has the advantage of no radiation, increased spatial resolution (compared to nuclear techniques), and provides functional information. Essentially, the concept of myocardial perfusion imaging is simply the relative changes in myocardial signal intensity are assessed during a bolus administration of gadolinium contrast agent under both pharmacological stress (typically either regadenoson, adenosine, or much less commonly in pediatrics, dipyridamole) and physical stress such as exercise on an MRI-compatible supine ergometer and at rest. The contrast agent causes increased myocardial signal intensity in proportion to the amount of contrast agent passing through each region of myocardium which is, in turn, proportional to the amount of coronary blood flow. Normally perfused myocardium will have a more rapid and intense signal increase under pharmacologic stress as compared with rest, while areas supplied by coronary arteries with flow-limiting stenosis will have slower and less intense rise in signal intensity under stress conditions.

Myocardial perfusion imaging is generally performed as a T_1-weighted, segmented gradient-echo or steady-state free precession implementation. T_1 weighting is improved by a preparatory radiofrequency pulse at the beginning of the sequence; inversion recovery preparation has been utilized and provides the greatest contrast between normal and abnormal myocardium; however, because it is sensitive to arrhythmias, a saturation recovery preparatory pulse is now generally utilized that renders the magnetization insensitive to arrhythmias, and allowing quantitative assessment of results. In general, a stack of 3–6 short axis slices and, if possible, 4-chamber and long axis views of the ventricle (depending upon the disease and parameters chosen) are acquired under pharmacologic stress and then, approximately 15–20 min later, repeated at rest which is finally followed by delayed enhancement (see above) 10 min afterwards. Images are obtained for every beat or every other beat, depending on the sequence.

Analysis of the images depend upon the relative changes in signal intensity (either qualitative or semiquantitative) to assess for ischemia. Qualitatively, the assessment is performed as a cine and visual analysis is performed of the relative signal intensity in regions of myocardium; a reduced rate of increase in signal intensity or an absolute decrease in signal intensity relative to normal myocardium is abnormal. This can be either because of (a) hypoperfusion, (b) infarction, or (c) artifact. To determine the difference between these, stress and rest perfusion images are combined with delayed enhancement imaging. If the region of abnormal signal intensity corresponds to infarcted regions of the ventricle, then the reason for abnormal signal intensity is obvious. If it does not, then hypoperfusion and ischemia are the reason if the stress images show the defect and the rest images do not. It is most likely an artifact if both rest and stress images show the defect (but not always) and there is a typical artifact pattern (susceptibility artifact, Gibbs ringing, or excessive motion of the heart). The visual analysis is simple, relatively fast, and has comparable sensitivity and specificity to nuclear techniques. Semiquantitative and quantitative approaches are more time-consuming which make it less suitable for routine use; however, it is used in some centers and in some studies, which improved the accuracy over visual analysis. Quantitative assessment is complex using an input arterial function; however, automated quantitative perfusion imaging is being tested at some centers [86].

Perfusion CMR has been investigated since 1990; however, because of software and hardware advances, it has gained the greatest clinical use since ~2000. Since that time, there have been numerous single-center studies demonstrating its clinical utility and accuracy. There is limited data in the literature; unfortunately, in patients with congenital heart disease, however, alternatives such as nuclear imaging and cardiac catheterization expose children to radiation; using CMR myocardial perfusion imaging for some of these applications has obvious potential benefits. Potential applications in congenital heart disease include patients who have had coronary artery manipulation (e.g., transposition of the great arteries after arterial switch procedure or patients after the Ross procedure), anomalous coronary arteries, assessment of cardiac tumors, and Kawasaki's disease. Perfusion imaging is safe in pediatrics and this data was recently published in the past few years [87].

1.9.3 Myocardial Strain

Relatively recently, in the echocardiographic world, strain has become a hot topic; however, it should be noted the CMR was the first noninvasive imaging modality to assess strain. As early as 1988, Zerhouni et al. demonstrated how to use "myocardial tagging" to assess strain in the heart [88]. Other

methodologies have since developed such as "displacement encoding with stimulated echoes (DENSE)" [89], strain encoded CMR or "SENC" [90], and myocardial velocimetry using phase contrast techniques (see below) [91]. These are dedicated sequences for strain. Relatively recently, feature and tissue tracking can be applied to regular cine imaging to extract global, longitudinal, and radial strains [92–95]. Regional strain has been found to inversely correlate with measures of ventricular fibrosis [96]. Regional strain can be utilized to assess for dyssynchrony as well.

A couple of protocols for specific disease states are worth mentioning that use the techniques noted above.

1.9.4 Tumor/Mass Characterization (Figs. 1.8, 1.9, and 1.10)

Characterization of tumors and masses on CMR is very useful as a high likelihood of what the mass is can be obtained. Many cardiac tumors and masses can be differentiated from each other by their tissue characteristics as well as their location, symptoms, and the patient's age. For example, a lipoma will be signal intense on T_1-weighted images and become signal poor after fat saturation. A hemangioma will become signal intense during perfusion imaging and may be indistinguishable from the ventricular cavity on the image which is one of its characteristics. Tumor characterization by CMR includes T_1- and T_2-weighted images, images with fat saturation, gradient echo imaging, perfusion (e.g., for hemangiomas), delayed enhancement imaging, T_1-weighted images after gadolinium administration, and myocardial tagging. If time permits, functional imaging can be used to assess for effects of the tumor such as obstruction to flow and decreased cardiac output. A multicenter pediatric registry of tumors in children and their characteristics was published in 2011 [97].

1.9.5 Arrhythmogenic Right Ventricular Dysplasia

With fatty or fibrofatty replacement of myocardium, mostly of the right ventricle, arrhythmias can generally result (e.g., left bundle branch block tachycardia). In its severest form, the right ventricle can become dilated and function poorly with dyskinetic wall regions. In addition, there can be right ventricular conduction delay on ECG, inverted T waves, and Epsilon waves. As imaging is only one of multiple criteria in the 2010 Task Force manuscript, it cannot be utilized in and of itself to make a diagnosis but must be combined with other criteria [98]. There are criteria for arrhythmogenic right ventricular dysplasia in adults and have been utilized successfully; however, when applied to the pediatric population, there is a question of how useful it truly is [99]. The CMR findings in adults with arrhythmogenic right ventricular dysplasia vary from study to study but in general, there is (1) fatty substitution of the myocardium, (2) ectasia of the RVOT, (3) dyskinetic bulges or dyskinesia of RV wall motion, (4) a dilated RV, (5) a dilated RA, and (6) fixed RV wall thinning with decreased RV wall thickening. The protocol includes simply cine for ventricular function to assess wall motion and ventricular volumes, phase-encoded velocity mapping of the aortic and pulmonary valves, and delayed enhancement which was shown to be helpful in a couple of studies; solely right ventricular volume and regional wall abnormalities are in the 2010 Task Force criteria. T_1-weighted imaging is not utilized anymore for evidence of fatty substitution of the myocardium by CMR; it is not one of the criteria and must be done by biopsy.

1.9.6 Other Techniques

Because of space limitations, techniques which will not be discussed in this chapter but the reader should be aware of are:

- XMR—the combination of CMR and cardiac catheterization
- Interventional CMR—performing intervention in the CMR suite
- Exercise CMR—utilizing a "CMR-friendly" exercise bicycle or other technique to obtain ventricular function and flow parameters during exercise
- Fetal CMR—utilizing CMR for evaluation of the heart in utero
- BOLD and other T_2 techniques for oxygen saturation
- Details of CMR at 3 T as applied to pediatrics and congenital heart disease
- Although it was mentioned above details of four-dimensional velocity mapping (Fig. 1.26)

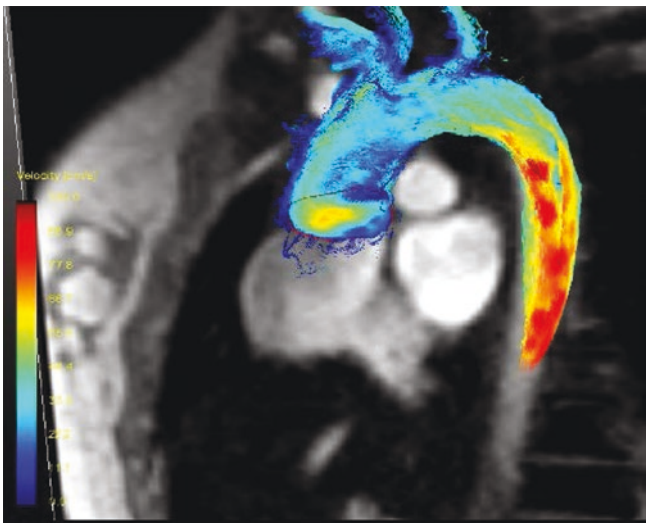

Fig. 1.26 Four-dimensional flow in the candy cane view of the normal aorta by utilizing a stack of 3-dimensional phase-encoded velocity maps. Color code of the velocity is in the lower left of the image

References

1. Ridgway JP. Cardiovascular magnetic resonance physics for clinicians: part I. J Cardiovasc Magn Reson. 2010;12(1):71.
2. Campbell-Washburn AE, Ramasawmy R, Restivo MC, et al. Opportunities in interventional and diagnostic imaging by using high-performance low-field-strength MRI. Radiology. 2019;293:384–93.
3. Bandettini WP, Shanbhag SM, Mancini C, et al. A comparison of cine CMR imaging at 0.55 T and 1.5 T. J Cardiovasc Magn Reson. 2020;22:37.
4. Simonetti OP, Finn JP, White RD, Laub G, Henry DA. "Black blood" T2-weighted inversion-recovery MR imaging of the heart. Radiology. 1996;199:49–57.
5. Carr JC, Simonetti OP, Bundy JM, Li D, Pereles S, Finn JP. Cine MR angiography of the heart with segmented true fast imaging with steady-state precession. Radiology. 2001;219:828–34.
6. Fogel MA, Gupta K, Baxter MS, Weinberg PM, Haselgrove J, Hoffman EA. Biomechanics of the deconditioned left ventricle. Am J Physiol Heart Circ Physiol. 1996;40:H1193–206.
7. Fogel MA, Gupta KB, Weinberg PW, Hoffman EA. Regional wall motion and strain analysis across stages of Fontan reconstruction by magnetic resonance tagging. Am J Physiol Heart Circ Physiol. 1995;38:H1132–52.
8. Fogel MA, Weinberg PM, Fellows KE, Hoffman EA. A Study in ventricular - ventricular interaction: single right ventricles compared with systemic right ventricles in a dual chambered circulation. Circulation. 1995;92:219–30.
9. Young AA, Axel L, Dougherty L, et al. Validation of tagging with MR imaging to estimate material deformation. Radiology. 1993;188:101–8.
10. Menteer J, Weinberg PM, Fogel MA. Quantifying regional right ventricular function in tetralogy of fallot. J Cardiovasc Magn Reson. 2005;7:753–61.
11. Shankaranarayanan A, Simonetti OP, Laub G, Lewin JS, Duerk JL. Segmented k-space and real-time cardiac cine MR imaging with radial trajectories. Radiology. 2001;221:827–36.
12. Li F. Golden-angle radial MRI: basics, advances, and applications. J Magn Reson Imaging. 2022;56:45–62.
13. Atkinson DJ, Edelman RR. Cineangiography of the heart in a single breath hold with a segmented turboFLASH sequence. Radiology. 1991;178:357–60.
14. Xue H, Kellman P, Larocca G, et al. High spatial and temporal resolution retrospective cine cardiovascular magnetic resonance from shortened free breathing real-time acquisitions. J Cardiovasc Magn Reson. 2013;15:102.
15. Pruessmann KP, Weiger M, Scheidegger MB, Boesiger P. SENSE: sensitivity encoding for fast MRI. Magn Reson Med. 1999;42:952–62.
16. Kellman P, Epstein FH, McVeigh ER. Adaptive sensitivity encoding incorporating temporal filtering (TSENSE). Magn Reson Med. 2001;45:846–52.
17. Jaspan ON, Fleysher R, Lipton ML. Compressed sensing MRI: a review of the clinical literature. Br J Radiol. 2015;88:20150487.
18. Heerfordt J, Whitehead KK, Bastiaansen JAM, et al. A SImilarity-driven Multi-dimensional Binning Algorithm (SIMBA) for free-running motion-suppressed whole-heart MRA. Magn Reson Med. 2021;86:213–29.
19. Cheng JY, Hanneman K, Zhang T, et al. Comprehensive motion-compensated highly-accelerated 4D flow MRI with ferumoxytol enhancement for pediatric congenital heart disease. J Magn Reson Imaging. 2016;43:1355–68.
20. Nguyen KL, Ghosh R, Griffin L, et al. Four-dimensional multiphase, steady-state MRI with ferumoxytol enhancement: early multicenter feasibility in pediatric congenital heart disease. Radiology. 2021;300:162–73.
21. Nguyen KL, Yoshida T, Kathuria-Prakash N, et al. Multicenter safety results for off-label diagnostic use of ferumoxytol in MRI. Radiology. 2019;293:554–64.
22. Fogel MA, Pawlowski TW, Harris MA, et al. Comparison and usefulness of cardiac magnetic resonance versus computed tomography in infants six months of age or younger with aortic arch anomalies without deep sedation or anesthesia. Am J Cardiol. 2011;108:120–5.
23. Shariat M, Mertens L, Seed M, et al. Utility of feed-and-sleep cardiovascular magnetic resonance in young infants with complex cardiovascular disease. Pediatr Cardiol. 2015;36:809–12.
24. Malviya S, Voepel-Lewis T, Eldevik OP, Rockwell DT, Wong JH, Tait AR. Sedation and general anaesthesia in children undergoing MRI and CT: adverse events and outcomes. Br J Aneasth. 2000;84:743–8.
25. Fogel MA, Weinberg P, Parave E, Harris C, Montenegro L, Concepcion M. Safety and efficacy of deep sedation in infants, children and adolescents undergoing cardiac magnetic resonance. J Pediatr. 2008;152:534–9.
26. Malviya S, Voepel-Lewis T, Tait AR. Adverse events and risk factors associated with the sedation of children by nonanesthesiologists. Anesth Analg. 1997;85:1207–13.
27. Bluemke DA, Breiter SN. Sedation procedures in MR imaging: safety, effectiveness, and nursing effect on examinations. Radiology. 2000;216:645–52.
28. Shepherd JK, Hall-Craggs MA, Finn JP, Bingham RM. Sedation in children scanned with high-field magnetic resonance: experience at the Hospital for Sick Children, Great Ormond Street. Br J Radiol. 1990;63:794–7.
29. Vade A, Sukhani R, Dolenga M, Habisohn-Schuck C. Choral hydrate sedation of children undergoing CT and MR imaging: safety as judged by American Academy of Pediatrics guidelines. Am J Roentgenol. 1995;165:905–9.
30. Volle E, Park W, Kaufmann HJ. MRI examination and monitoring of pediatric patients under sedation. Pediatr Radiol. 1996;26:280–1.
31. Lawson GR. Sedation of children for magnetic resonance imaging. Arch Dis Child. 2000;82:150–4.
32. Didier D, Ratib O, Beghetti M, et al. Morphologic and functional evaluation of congenital heart disease by magnetic resonance imaging. J Magn Reson Imaging. 1999;10:639–55.
33. Nayak KS, Hargreaves BA, Hu BS, Nishimura DG, Pauly JM, Meyer CH. Spiral balanced steady-state free precession cardiac imaging. Magn Reson Med. 2005;53:1468–73.
34. Scheffler K, Lehnhardt S. Principles and applications of balanced SSFP techniques. Eur Radiol. 2003;13:2409–18.
35. Lorenz CH, Walker ES, Morgan VL, Klein SS, Graham TP Jr. Normal human right and left ventricular mass, systolic function, and gender differences by cine magnetic resonance imaging. J Cardiovasc Magn Reson. 1999;1:7–21.
36. Marcus JT, DeWaal LK, Götte MJ, van der Geest RJ, Heethaar RM, Van Rossum AC. MRI-derived left ventricular function parameters and mass in healthy young adults: relation with gender and body size. Int J Card Imaging. 1999;15:411–9.
37. Sandstede J, Lipke C, Beer M, Hofmann S, Pabst T, Kenn W, Neubauer S, Hahn D. Age- and gender-specific differences in left and right ventricular cardiac function and mass determined by cine magnetic resonance imaging. Eur Radiol. 2000;10:438–42.
38. Mostbeck GH, Caputo GR, Higgins CB. MR measurement of blood flow in the cardiovascular system. AJR Am J Roentgenol. 1992;159:453–61.
39. Chatzimavroudis GP, Oshinski JN, Franch RH, Walker PG, Yoganathan AP, Pettigrew RI. Evaluation of the precision of magnetic resonance phase velocity mapping for blood flow measurements. J Cardiovasc Magn Reson. 2001;3:11–9.

40. Brenner LD, Caputo GR, Mostbeck G, et al. Quantification of left-to-right atrial shunts with velocity-encoded cine nuclear magnetic resonance imaging. J Am Coll Cardiol. 1992;20:1246–50.
41. Rebergen SA, Niezen RA, Helbing WA, et al. Cine gradient-echo MR imaging and MR velocity mapping in the evaluation of congenital heart disease. Radiographics. 1996;16:467–81.
42. John AS, Dill T, Brandt RR, Rau M, Ricken W, Bachmann G, Hamm CW. Magnetic resonance to assess the aortic valve area in aortic stenosis: how does it compare to current diagnostic standards? J Am Coll Cardiol. 2003;42:519–26.
43. Schlosser T, Malyar N, Jochims M, Breuckmann F, Hunold P, Bruder O, Erbel R, Barkhausen J. Quantification of aortic valve stenosis in MRI-comparison of steady-state free precession and fast low-angle shot sequences. Eur Radiol. 2007;17:1284–90.
44. Westenberg JJ, Roes SD, Ajmone Marsan N, Binnendijk NM, Doornbos J, Bax JJ, Reiber JH, de Roos A, van der Geest RJ. Mitral valve and tricuspid valve blood flow: accurate quantification with 3D velocity-encoded MR imaging with retrospective valve tracking. Radiology. 2008;249:792.
45. Firmin DN, Nayler GL, Klipstein RH, Underwood SR, Rees RS, Longmore DB. In vivo validation of MR velocity imaging. J Comput Assist Tomogr. 1987;11:751–6.
46. Caputo GR, Kondo C, Masui T, Geraci SJ, Foster E, O'Sullivan MM, Higgins CB. Right and left lung perfusion: *in vitro* and *in vivo* validation with oblique-angle, velocity-encoded cine MR imaging. Radiology. 1991;180:693–8.
47. Markl M, Kilner PJ, Ebbers T. Comprehensive 4D velocity mapping of the heart and great vessels by cardiovascular magnetic resonance. J Cardiovasc Magn Reson. 2011;13:7.
48. Markl M, Frydrychowicz A, Kozerke S, Hope M, Wieben O. 4D flow MRI. J Magn Reson Imaging. 2012;36:1015–36.
49. Cheng JY, Zhang T, Alley MT, Uecker M, Lustig M, Pauly JM, Vasanawala SS. Comprehensive multi-dimensional MRI for the simultaneous assessment of cardiopulmonary anatomy and physiology. Sci Rep. 2017;7:5330.
50. Rebergen SA, Chin JGJ, Ottenkamp J, van der Wall EE, de Roos A. Pulmonary regurgitation in the late postoperative follow-up of tetralogy of Fallot: volumetric quantification by MR velocity mapping. Circulation. 1993;88:2257–66.
51. Beerbaum P, Korperich H, Barth P, et al. Non-invasive quantification of left-to-right shunt in pediatric patients. Phase-contrast cine magnetic resonance imaging compared with invasive oximetry. Circulation. 2001;103:2476–82.
52. Harris MA, Weinberg PM, Whitehead KK, Fogel MA. Usefulness of branch pulmonary artery regurgitant fraction to estimate the relative right and left pulmonary vascular resistances in congenital heart disease. Am J Cardiol. 2005;95:1514–7.
53. Steffens JC, Bourne MW, Sakuma H, O'Sullivan M, Higgins CB. Quantification of collateral blood flow in coarctation of the aorta by velocity encoded cine magnetic resonance imaging. Circulation. 1994;90(2):937–43.
54. Whitehead KK, Gillespie MJ, Harris MA, Fogel MA, Rome JJ. Noninvasive quantification of systemic to pulmonary collateral flow: a major source of inefficiency in patients with superior cavopulmonary connections. Circ Cardiovasc Imag. 2009;2:405–11. Epub 2009 Jul 8.
55. Tzemos N, Therrien J, Yip J, Thanassoulis G, Tremblay S, Jamorski MT, Webb GD, Siu SC. Outcomes in adults with bicuspid aortic valves. JAMA. 2008;300:1317–25.
56. Gleeson TG, Mwangi I, Horgan SJ, Cradock A, Fitzpatrick P, Murray JG. Steady-state free-precession (SSFP) cine MRI in distinguishing normal and bicuspid aortic valves. J Magn Reson Imaging. 2008;28:873–8.
57. Vasanawala SS, Hanneman K, Alley MT, Hsiao A. Congenital heart disease assessment with 4D flow MRI. J Magn Reson Imaging. 2015;42:870–86.
58. Houriez-Gombaud-Saintonge S, Mousseaux E, Bargiotas I, De Cesare A, Dietenbeck T, Bouaou K, Redheuil A, Soulat G, Giron A, Gencer U, Craiem D, Messas E, Bollache E, Chenoune Y, Kachenoura N. Comparison of different methods for the estimation of aortic pulse wave velocity from 4D flow cardiovascular magnetic resonance. J Cardiovasc Magn Reson. 2019;21:75.
59. Rengier F, Delles M, Eichhorn J, et al. Noninvasive pressure difference mapping derived from 4D flow MRI in patients with unrepaired and repaired aortic coarctation. Cardiovasc Diagn Ther. 2014;4:97–103.
60. Rodríguez-Palomares JF, Dux-Santoy L, Guala A, et al. Aortic flow patterns and wall shear stress maps by 4D-flow cardiovascular magnetic resonance in the assessment of aortic dilatation in bicuspid aortic valve disease. J Cardiovasc Magn Reson. 2018;20:28.
61. Kamphuis VP, Elbaz MSM, van den Boogaard PJ, et al. Disproportionate intraventricular viscous energy loss in Fontan patients: analysis by 4D flow MRI. Eur Heart J Cardiovasc Imaging. 2019;20:323–33.
62. Tandon A, Hashemi S, Parks WJ, Kelleman MS, Sallee D, Slesnick TC. Improved high-resolution pediatric vascular cardiovascular magnetic resonance with gadofosveset-enhanced 3D respiratory navigated, inversion recovery prepared gradient echo readout imaging compared to 3D balanced steady-state free precession readout imaging. J Cardiovasc Magn Reson. 2017;18:74.
63. Piccini D, Littmann A, Nielles-Vallespin S, Zenge MO. Respiratory self-navigation for whole-heart bright-blood coronary MRI: methods for robust isolation and automatic segmentation of the blood pool. Magn Reson Med. 2012;68:571–9.
64. Kwong RY, Korlakunta H. Diagnostic and prognostic value of cardiac magnetic resonance imaging in assessing myocardial viability. Top Magn Reson Imaging. 2008;19:15–24.
65. Kim RJ, Wu E, Rafael A, et al. The use of contrast-enhanced magnetic resonance imaging to identify reversible myocardial dysfunction. N Engl J Med. 2000;343:1445–53.
66. Wu E, Judd RM, Vargas JD, Klocke FJ, Bonow RO, Kim RJ. Visualisation of presence, location, and transmural extent of healed Q-wave and non-Q-wave myocardial infarction. Lancet. 2001;357:21–8.
67. Simonetti OP, Kim RJ, Fieno DS, et al. An improved MR imaging technique for the visualization of myocardial infarction. Radiology. 2001;218:215–23.
68. Moon JC, Reed E, Sheppard MN, et al. The histologic basis of late gadolinium enhancement cardiovascular magnetic resonance in hypertrophic cardiomyopathy. J Am Coll Cardiol. 2004;43:2260–4.
69. Babu-Narayan SV, Goktekin O, Moon JC, et al. Late gadolinium enhancement cardiovascular magnetic resonance of the systemic right ventricle in adults with previous atrial redirection surgery for transposition of the great arteries. Circulation. 2005;111:2091–8.
70. Babu-Narayan SV, Kilner PJ, Li W, et al. Ventricular fibrosis suggested by cardiovascular magnetic resonance in adults with repaired tetralogy of fallot and its relationship to adverse markers of clinical outcome. Circulation. 2006;113:405–13.
71. Wald RM, Haber I, Wald R, Valente AM, Powell AJ, Geva T. Effects of regional dysfunction and late gadolinium enhancement on global right ventricular function and exercise capacity in patients with repaired tetralogy of fallot. Circulation. 2009;119:1370–7.
72. Choudhury L, Mahrholdt G, Wagner A, et al. Myocardial scarring in asymptomatic or mildly symptomatic patients with hypertrophic cardiomyopathy. J Am Coll Cardiol. 2002;40:2156–64.
73. Teraoka K, Hirano M, Ookubo H, et al. Delayed contrast enhancement of MRI in hypertrophic cardiomyopathy. Magn Reson Imaging. 2004;22:155–61.

74. Jcc M, McKenna W, McCrohon JA, Elliott PM, Smith GC, Pennell DJ. Toward clinical risk assessment in hypertrophic cardiomyopathy with gadolinium cardiovascular magnetic resonance. J Am Coll Cardiol. 2003;41:1561–7.
75. Taylor AJ, Salerno M, Dharmakumar R, Jerosch-Herold M. T1 mapping: basic techniques and clinical applications. J Am Coll Cardiol Img. 2016;9:67–81.
76. O'Brien A, Gil KE, Varghese J, et al. T2 mapping in myocardial disease: a comprehensive review. J Cardiovasc Magn Reson. 2022;24:33.
77. Triadyaksa P, Oudkerk M, Sijens PE. Cardiac T2* mapping: techniques and clinical applications. J Magn Reson Imaging. 2020;52:1340–51.
78. Treibel TA, Fontana M, Maestrini V, et al. Automatic measurement of the myocardial interstitium: synthetic extracellular volume quantification without hematocrit sampling. J Am Coll Cardiol Img. 2016;9:54–63.
79. Raucci FJ, Parra DA, Christensen JT, et al. Synthetic hematocrit derived from the longitudinal relaxation of blood can lead to clinically significant errors in measurement of extracellular volume fraction in pediatric and young adult patients. J Cardiovasc Magn Reson. 2017;19:58.
80. Kozak MF, Redington A, Yoo SJ, Seed M, Greiser A, Grosse-Wortmann L. Diffuse myocardial fibrosis following tetralogy of Fallot repair: a T1 mapping cardiac magnetic resonance study. Pediatr Radiol. 2014;44:403–9.
81. Yim D, Riesenkampff E, Caro-Dominguez P, et al. Assessment of diffuse ventricular myocardial fibrosis using native T1 in children with repaired tetralogy of Fallot. Circ Cardiovasc Imag. 2017;10:e005695.
82. Broberg CS, Huang J, Hogberg I, et al. Diffuse LV myocardial fibrosis and its clinical associations in adults with repaired tetralogy of fallot. J Am Coll Cardiol Img. 2016;9:86–7.
83. Ferreira VM, Schulz-Menger J, Holmvang G, Kramer CM, Carbone I, Sechtem U, et al. Cardiovascular magnetic resonance in nonischemic myocardial inflammation: expert recommendations. J Am Coll Cardiol. 2018;72:3158–76.
84. Danias PG, Stuber M, Botnar RM, Kissinger KV, Edelman RR, Manning WJ. Relationship between motion of coronary arteries and diaphragm during free breathing: lessons from real-time MR imaging. AJR Am J Roentgenol. 1999;172:1061–5.
85. Oncel D, Oncel G, Türkoğlu I. Accuracy of MR coronary angiography in the evaluation of coronary artery stenosis. Diagn Interv Radiol. 2008;14:153–8.
86. Xue H, Davies RH, Brown LAE, et al. Automated inline analysis of myocardial perfusion MRI with deep learning. Radiol Artif Intell. 2020;2:e 200009.
87. Biko D, Collins RT, Partington S, Harris MA, Whitehead KK, Keller M, Fogel MA. Magnetic resonance myocardial perfusion imaging: safety and indications in pediatrics and young adults. Pediatr Cardiol. 2018;39:275–82.
88. Zerhouni EA, Parish DM, Rogers WJ, Yang A, Shapiro EP. Human heart tagging with MR imaging: a method for noninvasive assessment of myocardial motion. Radiology. 1988;169:59–63.
89. Zhong X, Spottiswoode BS, Meyer CH, et al. Imaging three-dimensional myocardial mechanics using navigator-gated volumetric spiral cine DENSE MRI. Magn Reson Med. 2010;64:1089–97.
90. Neizel M, Lossnitzer D, Korosoglou G, et al. Strain-encoded (SENC) magnetic resonance imaging to evaluate regional heterogeneity of myocardial strain in healthy volunteers: comparison with conventional tagging. J Magn Reson Imaging. 2009;29:99–105.
91. Petersen SE, Jung BA, Wiesmann F, et al. Myocardial tissue phase mapping with cine phase-contrast MR imaging: regional wall motion analysis in healthy volunteers. Radiology. 2006;238:816–26.
92. Wehne GJ, Jing L, Haggerty CM, Suever JD, Chen J, Hamlet SM, Feindt JA, Mojsejenko WD, Fogel MA, Fornwalt BK. Comparison of left ventricular strains and torsion derived from feature tracking and DENSE. J Cardiovasc Magn Reson. 2018;20:63.
93. Muser D, Castro SA, Santangeli P, Nucifora G. Clinical applications of feature-tracking cardiac magnetic resonance imaging. World J Cardiol. 2018;10:210–21.
94. Schuster A, Hor KN, Kowallick JT, Beerbaum P, Kutty S. Cardiovascular magnetic resonance myocardial feature tracking. Concepts and clinical applications. Circ Cardiovasc Imag. 2016;9:e004077.
95. Sobh DM, Batouty NM, Tawfik AM, et al. Left ventricular strain analysis by tissue tracking - cardiac magnetic resonance for early detection of cardiac dysfunction in children with end-stage renal disease. J Mag Reson Med. 2021;54:1476–85.
96. Haggerty C, Suever J, Pulenthiran A, Mejia-Spiegeler A, Wehner G, Jing L, Charnigo R, Fornwalt B, Fogel M. Association between left ventricular mechanics and diffuse myocardial fibrosis in patients with repaired tetralogy of fallot: a cross-sectional study. J Cardiovasc Magn Reson. 2017;19:100.
97. Beroukhim RS, Prakash A, Buechel ERV, Cava JR, Dorfman AL, Festa P, et al. Characterization of cardiac tumors in children by cardiovascular magnetic resonance imaging: a multicenter experience. J Am Coll Cardiol. 2011;58:1044–54.
98. Marcus FI, McKenna WJ, Sherrill D, et al. Diagnosis of arrhythmogenic right ventricular cardiomyopathy/dysplasia. Proposed modification of the task force criteria. Circulation. 2010;121:1533–41.
99. Fogel MA, Weinberg PM, Harris M, Rhodes L. Usefulness of magnetic resonance imaging for the diagnosis of right ventricular dysplasia in children. Am J Cardiol. 2006;97(8):1232–7.